SPECIAL TOPIC — Phononics and phonon engineering

A polaron theory of quantum thermal transistor in nonequilibrium three-level systems*

Chen Wang(王晨)[1,†] and Da-Zhi Xu(徐大智)[2,‡]

[1] Department of Physics, Zhejiang Normal University, Jinhua 321004, China
[2] School of Physics and Center for Quantum Technology Research, Beijing Institute of Technology, Beijing 100081, China

(Received 26 March 2020; revised manuscript received 26 May 2020; accepted manuscript online 28 May 2020)

We investigate the quantum thermal transistor effect in nonequilibrium three-level systems by applying the polaron-transformed Redfield equation combined with full counting statistics. The steady state heat currents are obtained via this unified approach over a wide region of system–bath coupling, and can be analytically reduced to the Redfield and nonequilibrium noninteracting blip approximation results in the weak and strong coupling limits, respectively. A giant heat amplification phenomenon emerges in the strong system–bath coupling limit, where transitions mediated by the middle thermal bath are found to be crucial to unravel the underlying mechanism. Moreover, the heat amplification is also exhibited with moderate coupling strength, which can be properly explained within the polaron framework.

Keywords: quantum transport, open systems, nonequilibrium and irreversible thermodynamics, phonons or vibrational states in low-dimensional structures and nanoscale materials

PACS: 05.60.Gg, 03.65.Yz, 05.70.Ln, 63.22.−m **DOI:** 10.1088/1674-1056/ab973b

1. Introduction

According to the Clausius statement,[1] the heat flow from the hot source to the cold drain naturally occurs driven by the thermodynamic bias. Without violating this fundamental law of thermodynamics, great efforts have been paid to find other ways to conduct the heat flow.[2–8] Accompanying with the rapid progress in quantum technology, the control of heat flow becomes an increasingly important issue in quantum computation[9] and quantum measurement.[10,11]

The thermal transistor, one of the novel phenomena in quantum thermal transport, was initially proposed by B. Li and coworkers.[12,13] In particular, heat amplification and negative differential thermal conductance (NDTC) are considered as two main components of the thermal transistor. Heat amplification describes an effect within the three-terminal setup, that the tiny modification of the base current will dramatically change the current at the collector and emitter, which enables the efficient energy transport.[12] While the NDTC effect is characterized by the suppression of the heat flow with increase of temperature bias within the two-terminal setup.[14–16]

Later, the spin-based fully quantum thermal transistor was proposed by K. Joulain *et al.*,[17] which is composed by three coupled-qubits, each interacting with one individual thermal bath. The qubit–qubit interaction within the system is found to be crucial to exhibit the heat amplification. Consequently, the importance of the system nonlinearity and long-range interaction on the transistor effect has also been unraveled in various coupled-qubits systems.[18–20] Simultaneously, the strong qubit–bath interaction is revealed to be another key factor to cause giant heat amplification in the two- and three-qubits systems,[21,22] which also stems from the NDTC effect. Hence, NDTC is widely accepted as the crucial intergradient to realize the giant heat amplification. However, J. H. Jiang *et al.* pointed out that heat amplification can be realized via the inelastic transport process independent of NDTC.[23] Hence, basic questions are raised: Can these two types of heat amplification coexist in one quantum system? What is the underlying microscopic mechanism?

Very recently, a three-level quantum heat transistor was preliminarily investigated by S. H. Su *et al.*, which stressed the significant influence of quantum coherence on the heat amplification.[24] However, the calculations are based on the phenomenological Lindblad equation, which cannot be generalized to describe the heat transport beyond the weak system–bath coupling. Considering the scientific importance and extensive application of the nonequilibrium three-level systems,[25–33] it is intriguing to give a comprehensive picture of the heat transistor behavior. In particular, it is worthwhile to give a unified analysis on the effect of the system–bath interaction from the weak to strong coupling regimes on the heat amplification and NDTC.

In this paper, we devote to investigating quantum thermal transport in a quantum thermal transistor, which is composed

*Project supported by the National Natural Science Foundation of China (Grant Nos. 11704093 and 11705008) and Beijing Institute of Technology Research Fund Program for Young Scholars, China.

†Corresponding author. E-mail: wangchenyifang@gmail.com
‡Corresponding author. E-mail: dzxu@bit.edu.cn

by a three-level quantum system within the three-terminal setup (Fig. 1(a)) by applying the polaron-transformed Redfield equation (PTRE), detailed in Section 2. In Section 3, the heat currents are obtained from PTRE combined with full counting statistics (FCS),[34,35] and are reduced to the Redfield and nonequilibrium noninteracting blip approximation (NIBA) schemes.[36–39] In Subsection 4.1, the giant heat amplification is explored both with moderate and strong system–middle bath interaction strengths, and the finite heat amplification with inelastic-like process is analytically estimated in the weak system-middle bath coupling regime. The corresponding microscopic mechanisms are proposed. In Subsection 4.2, the negative differential thermal conductance is analyzed based on the two-terminal setup, where the cooperative contribution from thermal baths to exhibit NDTC is revealed to be crucial. Moreover, the NDTC is found at moderate system–middle bath coupling, which can not be explained by the Redfield equation. Finally, we give a concise summary in Section 5.

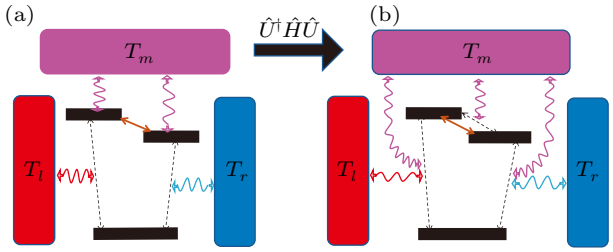

Fig. 1. Schematics of the nonequilbrium V-type three-level system in (a) the original framework and (b) the polaron framework. The three horizontal solid black lines represent the central three-level model ($|u\rangle$, $u = l, r, 0$), and the double-arrowed solid brown line shows the coherent tunneling between two excited states $|l\rangle$ and $|r\rangle$; the rectangular left red, top-middle purple, and right blue boxes describe three thermal baths, which are characterized by temperatures T_l, T_m, and T_r, respectively; the double-arrowed solid red, purple, and blue curves describe interactions between the system and thermal baths, and the double-arrowed dashed black lines describe transitions between different states assisted by phonons in the corresponding thermal bath.

2. Model and method

We first introduce the nonequilibrium three-level system and the framework of polaron transformation. Then, the polaron-transformed Redfield equation is applied to obtain the reduced system density matrix.

2.1. Nonequilibrium three-level system

The total Hamiltonian of the nonequilibrium three-level system interacting with three thermal baths shown in Fig. 1(a) is described as $\hat{H} = \hat{H}_s + \sum_{u=l,r,m}(\hat{H}_b^u + \hat{V}_u)$ with the units $\hbar = 1$ and $k_B = 1$. The quantum three-level system is expressed as[25,27–30]

$$\hat{H}_s = \varepsilon_0|0\rangle\langle 0| + \sum_{u=l,r} \varepsilon_u|u\rangle\langle u| + \Delta(|l\rangle\langle r| + \text{H.c.}), \tag{1}$$

where $|l(r)\rangle$ is the left (right) excited state with the occupation energy $\varepsilon_{l(r)}$, and $|0\rangle$ is the ground state with $\varepsilon_0 = 0$ for simplicity. Specifically, for $\varepsilon_{l(r)} > 0$, the three-level system corresponds to a V-type configuration. Whereas for $\varepsilon_{l(r)} < 0$, it corresponds to a Λ-type configuration with excited state $|0\rangle$ and ground states $|l\rangle$ and $|r\rangle$. It should be noted that the notions of V-type and Λ-type have already been used in quantum optics and quantum thermodynamics.[30,40,41] In the following, our work is based on the V-type system without losing any generality.

The Hamiltonian of the u-th $(u = l, m, r)$ thermal bath is described as $\hat{H}_b^u = \sum_k \omega_k \hat{b}_{k,u}^\dagger \hat{b}_{k,u}$, where $\hat{b}_{k,u}^\dagger$ ($\hat{b}_{k,u}$) creates (annihilates) one phonon in the u-th bath with the frequency ω_k. The interaction between the left (right) excited state and the corresponding bath is given by[29]

$$\hat{V}_u = (\hat{S}_u^\dagger + \text{H.c.}) \sum_k (g_{k,u}\hat{b}_{k,u}^\dagger + \text{H.c.}), \quad u = l, r, \tag{2}$$

with $\hat{S}_u^\dagger = |u\rangle\langle 0|$. Here, the state $|0\rangle$ only interacts with the left and right baths. While the quantum dissipation of the two excited states induced by the middle bath is modeled by a diagonal interaction,[24,28,29] which reads

$$\hat{V}_m = (|l\rangle\langle l| - |r\rangle\langle r|) \sum_k (g_{k,m}\hat{b}_{k,m}^\dagger + \text{H.c.}), \tag{3}$$

where $g_{k,u}$ is the system–bath coupling strength. The u-th thermal bath here is characterized by the spectral function $\Lambda_u(x) = 4\pi\sum_k |g_{k,u}|^2\delta(x - \omega_k)$, Here, the spectral functions are selected to have the super-Ohmic form $\Lambda_{l(r)}(x) = \pi\gamma_{l(r)}\frac{x^3}{\omega_c^2}\,\mathrm{e}^{-|x|/\omega_c}$ and $\Lambda_m(x) = \pi\alpha_m\frac{x^3}{\omega_c^2}\,\mathrm{e}^{-|x|/\omega_c}$, where $\gamma_{l(r)}$ and α_m are the coupling strengths corresponding to the $l(r)$-th bath and the m-th bath, and the cut-off frequency is ω_c. The super-Ohmic bath has been extensively included to investigate quantum dissipation[42,43] and quantum energy transport.[44–46]

In order to consider the interaction between the excited states and the middle bath beyond the weak coupling limit, we apply a canonical transformation [see Fig. 1(b)][36,37,43] $\hat{H}' = \hat{U}^\dagger\hat{H}\hat{U}$, with $\hat{U} = \exp[\mathrm{i}\hat{B}(|l\rangle\langle l| - |r\rangle\langle r|)]$ and the collective phonon momentum operator $\hat{B} = \mathrm{i}\sum_k(\frac{g_{k,m}}{\omega_k}\hat{b}_{k,m}^\dagger - \text{H.c.})$. The transformed Hamiltonian is given by $\hat{H}' = \hat{H}_s' + \sum_{u=l,m,r}(\hat{H}_b^u + \hat{V}_u')$. Specifically, the modified system Hamiltonian is given by[34,35]

$$\hat{H}_s' = \bar{\varepsilon}\hat{N} + \delta\varepsilon\hat{\sigma}_z + \eta\Delta\hat{\sigma}_x, \tag{4}$$

with the average occupation energy $\bar{\varepsilon} = (\varepsilon_l + \varepsilon_r)/2 - \sum_k |g_{k,m}|^2/\omega_k$, the energy bias $\delta\varepsilon = (\varepsilon_l - \varepsilon_r)/2$, the excitation number operator $\hat{N} = |l\rangle\langle l| + |r\rangle\langle r|$, the bias operator $\hat{\sigma}_z = |l\rangle\langle l| - |r\rangle\langle r|$, and the tunneling operator $\hat{\sigma}_x = |l\rangle\langle r| + |r\rangle\langle l|$. Here $\hat{N}$ can be re-expressed as $\hat{N} = \hat{I} - |0\rangle\langle 0|$ with $\hat{I}$ the unit operator in the space of the three-level system. It should be noted that the operators $\hat{\sigma}_a$ $(a = x, y, z)$ are not Pauli operators for $\hat{\sigma}_a^2 \neq \hat{I}$. The renormalization factor $\eta = \mathrm{Tr}_m\{\hat{\rho}_b^m\,\mathrm{e}^{\pm 2\mathrm{i}\hat{B}}\}/\mathrm{Tr}_m\{\hat{\rho}_b^m\}$, with $\mathrm{Tr}_m\{\}$ the trace over the middle bath, $\hat{\rho}_b^m = \mathrm{e}^{-\hat{H}_b^m/k_B T_m}$ thermal equilibrium state, and T_m the temperature of the middle bath. Then, the transformed

system Hamiltonian $\hat{H}_s'$ can be exactly solved as $\hat{H}_s'|\pm\rangle_\eta = E_\pm|\pm\rangle_\eta$, where the eigenstates are $|+\rangle_\eta = \cos\frac{\theta}{2}|l\rangle + \sin\frac{\theta}{2}|r\rangle$ and $|-\rangle_\eta = -\sin\frac{\theta}{2}|l\rangle + \cos\frac{\theta}{2}|r\rangle$, with $\tan\theta = \eta\Delta/\delta\varepsilon$ and the eigenvalues $E_\pm = \bar{\varepsilon}\pm\sqrt{(\delta\varepsilon)^2+(\eta\Delta)^2}$. The modified system-bath interactions are given by[34,35]

$$\hat{V}_m' = \Delta[\cos(2\hat{B}) - \eta]\hat{\sigma}_x + \Delta\sin(2\hat{B})\hat{\sigma}_y, \tag{5a}$$

$$\hat{V}_u' = (\mathrm{e}^{-\mathrm{i}\hat{B}_u}\hat{S}_u^\dagger + \mathrm{e}^{\mathrm{i}\hat{B}_u}\hat{S}_u)\sum_k (g_{k,u}\hat{b}_{k,u}^\dagger + g_{k,u}^*\hat{b}_{k,u}), \quad u = l,r, \tag{5b}$$

with $\hat{\sigma}_y = -\mathrm{i}(|l\rangle\langle r| - |r\rangle\langle l|)$, $\hat{B}_l = \hat{B}$, and $\hat{B}_r = -\hat{B}$. It should be noted that the factor η results from the renormalization of the dressed coherent tunneling between the two excited states, i.e., $\Delta\hat{U}^\dagger\hat{\sigma}_x\hat{U} = \eta\Delta\hat{\sigma}_x + \hat{V}_m'$, which makes the thermal average of $\hat{V}_m'$ vanish for arbitrary system–middle bath coupling strength.[34,43]

All the interaction terms $\hat{V}_u'$ $(u = l,m,r)$ of Eqs. (5a) and (5b) imply multi-phonon transferring processes. Specifically, $\hat{V}_m'$ involves multiple phonons absorption or emission accompanying the transition between the two excited states, which can be understood by the expansion $\cos(2\hat{B}) = \sum_{n=0}\frac{(2\hat{B})^{2n}}{(2n)!}$ and $\sin(2\hat{B}) = \sum_{n=0}\frac{(2\hat{B})^{2n+1}}{(2n+1)!}$. While the interaction between the left (right) bath phonon and the three-level system $\hat{V}_u'$ now involves the polaron effect embodied in the displacement operator $\exp(\pm\mathrm{i}\hat{B}_u)$ of the middle bath phonon modes.

2.2. Polaron-transformed Redfield equation

It can be easily verified that the thermal average of the modified interaction $\mathrm{Tr}_m\{\hat{\rho}_b^m\hat{V}_m'\}/\mathrm{Tr}_m\{\hat{\rho}_b^m\}$ is zero, which makes $\hat{V}_m'$ a properly perturbative term.[34] Therefore, we can apply the quantum master equation in the polaron frame to study the dynamics of the three-level system. Moreover, we assume the interaction between the system and the left (right) bath $\hat{V}_{l(r)}'$ is weak. Thus we can separately apply the perturbation theory with respect to the two terms in Eqs. (5a) and (5b). Accordingly, the PTRE based on the Born–Markov approximation can be written as

$$\frac{\mathrm{d}}{\mathrm{d}t}\hat{\rho}_s = -\mathrm{i}[\hat{H}_s', \hat{\rho}_s] + \sum_{u=l,m,r}\mathcal{L}_u[\hat{\rho}_s], \tag{6}$$

where $\hat{\rho}_s$ is the density operator of the three-level system. The m-th dissipator is specified as[34,35]

$$\mathcal{L}_m[\hat{\rho}_s] = \sum_{\alpha=x,y;\omega,\omega'}\gamma_\alpha(\omega')\big[\hat{P}_\alpha(\omega')\hat{\rho}_s\hat{P}_\alpha(\omega) - \hat{P}_\alpha(\omega)\hat{P}_\alpha(\omega')\hat{\rho}_s\big] + \mathrm{H.c.}, \tag{7}$$

where the dissipation rates between the two excited eigenstates are

$$\gamma_x(\omega) = \eta^2\Delta^2\int_0^\infty \mathrm{d}\tau\,\mathrm{e}^{\mathrm{i}\omega\tau}[\cosh\phi_m(\tau) - 1], \tag{8a}$$

$$\gamma_y(\omega) = \eta^2\Delta^2\int_0^\infty \mathrm{d}\tau\,\mathrm{e}^{\mathrm{i}\omega\tau}\sinh\phi_m(\tau), \tag{8b}$$

with the correlation phase

$$\phi_m(\tau) = 4\sum_k\left|\frac{g_{k,m}}{\omega_k}\right|^2\{\cos(\omega_k\tau)[2n_m(\omega_k)+1] - \mathrm{i}\sin(\omega_k\tau)\}.$$

The operators $\hat{P}_\alpha(\omega)$ $(\alpha = x,y)$ are the projective operators of the system eigenbasis, which are defined by $\hat{\sigma}_\alpha(-\tau) = \sum_\omega\hat{P}_\alpha(\omega)\mathrm{e}^{\mathrm{i}\omega\tau}$ with $\hat{P}_\alpha(-\omega) = \hat{P}_\alpha^\dagger(\omega)$.[47] The rate $\gamma_y(\omega)$ describes the transition between the two excited eigenstates $|\pm\rangle_\eta$ involving odd number of phonons from the middle thermal bath. The bath average phonon number is $n_u(\omega) = 1/[\exp(\omega/T_u) - 1]$, $u = r,l,m$, with T_u the temperature of the u-th bath. The approximated expression of the real part of $\gamma_y(\omega)$ to the first-order of ϕ_m reads $\mathrm{Re}[\gamma_y(\omega)] \approx 4\pi\eta^2\Delta^2\sum_k|\frac{g_{k,m}}{\omega_k}|^2[n_m(\omega_k)+1]\delta(\omega-\omega_k)$, which contains the sequential process of creating one phonon with frequency $\omega = \omega_k$ in the m-th bath. A direct consequence of the polaron transformation is that the dissipative rates $\gamma_x(\omega)$ and $\gamma_y(\omega)$ contain all the high-order terms of ϕ_m, which can be understood as the contribution of the multiple-phonon correlation. In the strong system–bath coupling strength regime, such high-order correlations should be properly incorporated in the evolution of the open quantum system.

Moreover, the dissipators associated with the left and right baths are given by

$$\begin{aligned}\mathcal{L}_u[\hat{\rho}_s] = \sum_{\omega,\omega'}\big[&\kappa_{u,-}(\omega')\hat{Q}_u(\omega')\hat{\rho}_s\hat{Q}_u^\dagger(\omega) \\ &+ \kappa_{u,+}(\omega')\hat{Q}_u^\dagger(\omega')\hat{\rho}_s\hat{Q}_u(\omega) \\ &- \kappa_{u,+}(\omega')\hat{Q}_u(\omega)\hat{Q}_u^\dagger(\omega')\hat{\rho}_s \\ &- \kappa_{u,-}(\omega')\hat{Q}_u^\dagger(\omega)\hat{Q}_u(\omega')\hat{\rho}_s\big] + \mathrm{H.c.},\end{aligned} \tag{9}$$

where the system part operators are defined by $\hat{S}_u(-\tau) = \sum_\omega\hat{Q}_u(\omega)\mathrm{e}^{\mathrm{i}\omega\tau}$,[48] and the dissipation rates are

$$\kappa_{u,+}(\omega) = \int_{-\infty}^{\infty}\frac{\mathrm{d}\omega_1}{4\pi}\Lambda_u(\omega_1)n_u(\omega_1)C_u(\omega_1-\omega), \tag{10a}$$

$$\kappa_{u,-}(\omega) = \int_{-\infty}^{\infty}\frac{\mathrm{d}\omega_1}{4\pi}\Lambda_u(\omega_1)[1+n_u(\omega_1)]C_u(-\omega_1+\omega). \tag{10b}$$

The phonon correlation function above is shown as $C_u(\omega) = \eta_u^2\int_0^\infty\mathrm{d}\tau\,\mathrm{e}^{\mathrm{i}\omega\tau}\mathrm{e}^{\phi_m(\tau)/4}$, where $\eta_u = \mathrm{Tr}_u\{\hat{\rho}_u\mathrm{e}^{\mathrm{i}\hat{B}}\}/\mathrm{Tr}_u\{\hat{\rho}_u\}$, with $\mathrm{Tr}_u\{\}$ the trace over the space of the u-th bath and $\hat{\rho}_u = \mathrm{e}^{-\hat{H}_b^u/k_\mathrm{B}T_u}$. The transition rates in Eqs. (10a) and (10b) demonstrate the joint contribution of the left (right) and the middle thermal baths on the nonequilibrium energy exchange. Specifically, $\kappa_{l(r),+}(\omega)$ describes the process that one phonon with the frequency ω_1 is emitted from the $l(r)$-th thermal bath to assist the excitation from $|0\rangle$ to the eigenstate with energy gap ω, and the resultant energy $\omega_1 - \omega > 0$ $(\omega_1 - \omega < 0)$ is released (absorbed) into (from) the m-th bath. While the rate $\kappa_{l(r),-}(\omega)$ shows the transition that one phonon with frequency ω_1 is absorbed by the $l(r)$-th thermal bath, and the three-level system is relaxed from the excited state with energy ω into $|0\rangle$.

For quantum heat transfer in the nonequilibrium spin-boson model, the polaron transformation and NIBA scheme

was firstly proposed by D. Segal and A. Nitzan,[36,37] where the NDTC was unraveled at strong system–bath coupling under the Marcus approximation. Moreover, D. Segal *et al.* combined the NIBA scheme with full counting statistics to investigate the heat current flucutuation.[38,39] Later, inspired by these works, the Redfield equation and NIBA limits were unified by introducing the PTRE embedded with full counting statistics.[34,35] It should be noted that in this work the perturbation treatment of the system–middle bath interaction by the polaron transformation is the same as done in previous works for the nonequilibrium spin-boson model, which makes it proper to arbitrarily tune the system–middle bath coupling strength.

However, for the dissipator in Eq. (9), it is found that though the system–left (right) bath coupling is weak, the energy exchange reflected by the transition rates in Eqs. (10a) and (10b) is cooperatively contributed by the left (right) bath and the middle bath. Such joint exchange process is apparently different from the sequential process in the nonequilibrium spin-boson model as treated by the Redfield method.[34,37] Therefore, we nontrivially extend the application of the polaron-transformed Redfield equation from the nonequilibrium spin-boson model[34,35] to the nonequilibrium three-level quantum system. This is the main technical point in the present work.

3. Steady state heat currents

We analyze steady state behaviors of heat currents via full counting statistics[33,49] by tuning the system–middle bath interaction in Fig. 2. The detail derivation of quantum master equation combined with full counting statistics and expressions of heat currents can be found in Appendix A. It is found that the currents are all significantly enhanced in the moderate coupling regime around $\alpha_m \in (0.5, 2)$, but are dramatically suppressed in both the strong and weak coupling limits. Moreover, the current flowing into the middle bath is more sensitive in response to the change of α_m. It can be seen that J_m begins to increase significantly when α_m is around 0.01, which is one order smaller than those of the other two currents. It should be noted that though the heat currents are seemly negligible in the weak system–middle bath coupling regime, they are actually nonzero (e.g., $J_l/\gamma = -0.00295$ with $\alpha_m = 0.001$).

The PTRE combined with FCS has been successfully introduced to investigate quantum thermal transport in the nonequilibrium spin-boson systems,[34,35,45] which is able to fully bridge the strong and weak system–bath coupling limits. While for the nonequilibrium three-level quantum system, it should admit that it is generally difficult to analytically obtain the expressions of steady state heat currents with arbitrary coupling strength α_m between two excited states and middle thermal bath. However, in the strong and weak coupling limits the NIBA approach and Redfield equation can adequately describe the steady state of the system, respectively.

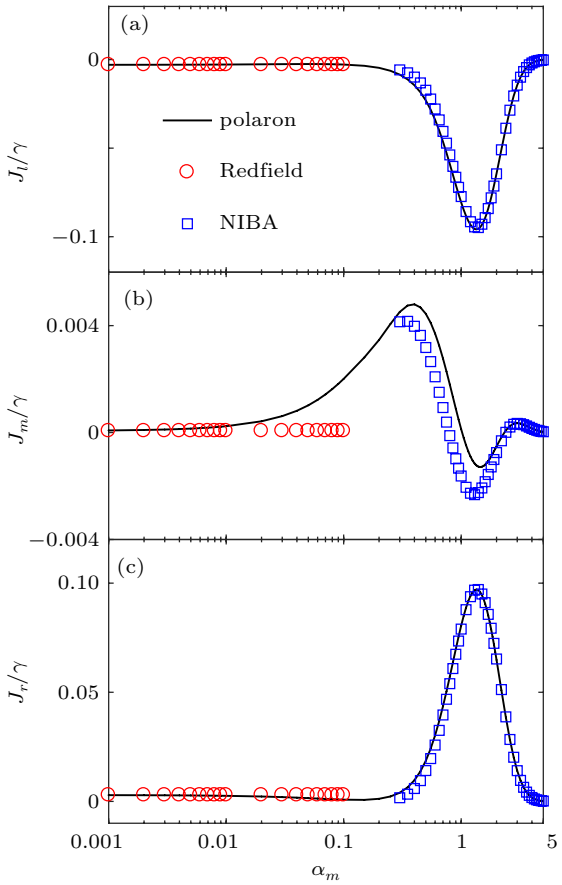

Fig. 2. Steady state heat currents (a) J_l/γ, (b) J_m/γ, and (c) J_r/γ as a function of the coupling strength α_m. The red circles are based on the Redfield scheme; the blue squares are based on the nonequilibrium noninteracting blip approximation (NIBA); the black solid line is calculated from the nonequilibrium polaron-transformed Redfield approach. The other parameters are given as $\varepsilon_l = 1.0$, $\varepsilon_r = 0.6$, $\Delta = 0.6$, $\gamma = 0.0002$, $\omega_c = 10$, $T_l = 2$, $T_m = 1.2$, and $T_r = 0.4$.

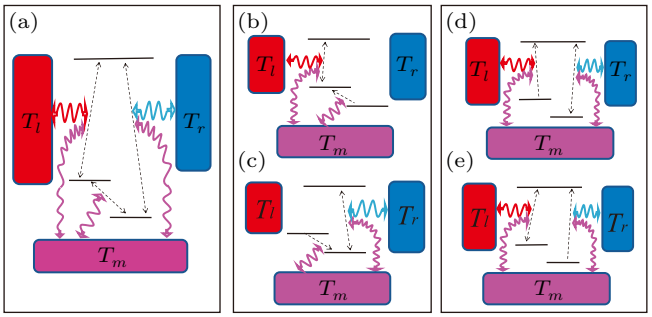

Fig. 3. (a) The globally cyclic transition contributed by the $G_l^{\pm}G_m^{\pm}G_r^{\mp}/\mathcal{A}$, and the locally conditional transitions contributed by (b) $G_m^{-}G_l^{+}G_l^{-}/\mathcal{A}$, (c) $G_m^{+}G_r^{+}G_r^{-}/\mathcal{A}$, (d) $G_r^{-}G_l^{+}G_l^{-}/\mathcal{A}$, and (e) $G_l^{-}G_r^{+}G_r^{-}/\mathcal{A}$ within the nonequilibrium NIBA scheme, respectively. The horizontal solid black line at top represents $|0\rangle$; two horizontal solid black lines at bottom describe renormalized energy levels $|l(r)\rangle$ with the energies $E_{l(r)} = \varepsilon_{l(r)} - \sum_k |g_{k,m}|^2/\omega_k$. The other symbols are the same as those in Fig. 1.

3.1. Strong coupling limit

In the strong coupling limit, the renormalization factor is dramatically suppressed, i.e., $\eta \ll 1$. The eigenstates are reduced to the localized ones $|+\rangle_\eta \approx |l\rangle$, $|-\rangle_\eta \approx |r\rangle$, and the renormalized energies become $E_u = (\varepsilon_u - \sum_k |g_{k,m}|^2/\omega_k)$, $u =$

l,r. As the renormalization energy $\sum_k |g_{k,m}|^2/\omega_k$ exceeds the bare energy ε_u, the configuration of the transformed three-level system becomes the Λ-type as shown in Fig. 3(a). Hence, the nonequilibrium PTRE is reduced to the NIBA scheme, which can be analytically solved (the details are given in Appendix B). Accordingly, the heat currents are explicitly given by

$$J_{l,\mathrm{NIBA}} = \frac{1}{\mathcal{A}}\big[(G_l^+G_m^+G_r^-\langle\omega\rangle_{l,+} - G_l^-G_m^-G_r^+\langle\omega\rangle_{l,-}) + (G_m^- + G_r^-)G_l^-G_l^+(\langle\omega\rangle_{l,+} - \langle\omega\rangle_{l,-})\big], \quad (11)$$

$$J_{r,\mathrm{NIBA}} = \frac{1}{\mathcal{A}}\big[(G_l^-G_m^-G_r^+\langle\omega\rangle_{r,+} - G_l^+G_m^+G_r^-\langle\omega\rangle_{r,-}) + (G_m^+ + G_l^-)G_r^+G_r^-(\langle\omega\rangle_{r,+} - \langle\omega\rangle_{r,-})\big], \quad (12)$$

and $J_m = -J_l - J_r$, where the coefficient is $\mathcal{A} = (G_m^+ + G_m^-)(G_l^+ + G_r^+) + G_m^+G_r^- + G_m^-G_l^- + G_l^-G_r^+ + G_r^-(G_l^+ + G_l^-)$, the transition rates are

$$G_m^\pm = \int_{-\infty}^{\infty} \mathrm{d}\tau \mathrm{e}^{\pm \mathrm{i}(\varepsilon_l-\varepsilon_r)\tau}\eta^2 \mathrm{e}^{\phi_m(\tau)}, \quad (13a)$$

$$G_u^+ = \frac{1}{4\pi}\int_{-\infty}^{\infty}\mathrm{d}\omega_1\Lambda_u(\omega_1)[1+n_u(\omega_1)] \times [C_u(-E_u-\omega_1)+\mathrm{H.c.}], \quad (13b)$$

$$G_u^- = \frac{1}{4\pi}\int_{-\infty}^{\infty}\mathrm{d}\omega_1\Lambda_u(\omega_1)n_u(\omega_1)[C_u(\omega_1+E_u)+\mathrm{H.c.}], \quad (13c)$$

and the average energies into the u-th thermal bath are

$$\langle\omega\rangle_{u,+} = \frac{1}{4\pi G_u^+}\int_{-\infty}^{\infty}\mathrm{d}\omega_1\omega_1\Lambda_u(\omega_1)[1+n_u(\omega_1)] \times [C_u(-E_u-\omega_1)+\mathrm{H.c.}], \quad (14a)$$

$$\langle\omega\rangle_{u,-} = \frac{1}{4\pi G_u^-}\int_{-\infty}^{\infty}\mathrm{d}\omega_1\omega_1\Lambda_u(\omega_1)n_u(\omega_1) \times [C_u(\omega_1+E_u)+\mathrm{H.c.}]. \quad (14b)$$

In the following, the subscript u only represents l or r without further declaration. The rates $G_u^\pm$ in Eqs. (13b) and (13c) are contributed by two physical processes. Take G_u^+ for example: (i) resonant energy relaxation from the state $|0\rangle$ to $|u\rangle$, with the energy E_u absorbed by the u-th thermal bath; (ii) off-resonant transport process, where the thermal baths show non-additive cooperation. As the three-level system releases energy E_u, part of the heat ω_1 is absorbed by the u-th bath, whereas the left energy $(-E_u-\omega_1)$ is consumed by the middle bath. Similarly, the rate G_u^- describes the reversed process of G_u^+.

The currents J_l and J_r in Eqs. (11) and (12) are contributed by three distinct types of thermal transport processes: (i) globally cyclic transition in Fig. 3(a), which is contributed by the cooperative rate $G_l^\pm G_m^\pm G_r^\mp/\mathcal{A}$ to carry the average energy $\langle\omega\rangle_{u,+}$ ($\langle\omega\rangle_{u,-}$) to (from) the u-th bath; (ii) local transition $|u\rangle\leftrightarrow|0\rangle$ mediated by the middle bath dependent rate $G_m^\pm$, which transfers the energy $\langle\omega\rangle_{u,+} - \langle\omega\rangle_{u,-}$. Figures 3(b) and 3(c) illustrate these transition processes characterized by the rates $G_m^-G_l^+G_l^-/\mathcal{A}$ and $G_m^+G_r^+G_r^-/\mathcal{A}$, respectively; (iii) local transition $|u\rangle\leftrightarrow|0\rangle$ mediated by the u-th bath dependent rate G_u^-, which is characterized by the rates $G_r^-G_l^+G_l^-/\mathcal{A}$ and $G_l^-G_r^+G_r^-/\mathcal{A}$ as illustrated in Figs. 3(d) and 3(e), respectively.

We compare the heat currents calculated by the nonequilibrium NIBA with the ones calculated by the PTRE in Fig. 2. It is found that $J_{l(r)}$ obtained by these two methods are consistent with each other in a wide regime of the coupling strength α_m. While J_m obtained from the nonequilibrium NIBA shows apparently disparity with the result of the PTRE, unless the coupling strength increases to the regime $\alpha_m \gtrsim 2$.

3.2. Weak coupling limit

In the weak coupling limit, the renormalization factor becomes $\eta \approx 1$. The counting parameter dependent transition rates defined in Eqs. (A5a) and (A5b) are simplified to $\mathrm{Re}[\kappa_{u,+}(\omega',\chi_u)] \approx \frac{1}{4}\Lambda(\omega')n_u(\omega')\mathrm{e}^{-\mathrm{i}\omega'\chi_u}$ and $\mathrm{Re}[\kappa_{u,-}(\omega',\chi_u)] \approx \frac{1}{4}\Lambda(\omega')[1+n_u(\omega')]\mathrm{e}^{\mathrm{i}\omega'\chi_u}$. Meanwhile, the transition rates in Eqs. (8a) and (8b) are reduced to $\mathrm{Re}[\gamma_x(\omega)] \approx 0$ and $\mathrm{Re}[\gamma_y(\omega)] \approx \frac{\Delta^2}{\omega^2}\Lambda_m(\omega)[1+n_m(\omega)]$, where we only keep the lowest order terms of the correlation phase $\phi_m(\tau)$. Then, the PTRE in Eq. (A3) is reduced to the seminal Redfield equation (see Appendix C). Consequently, the steady state currents are obtained as

$$J_l = \sum_{\xi=\pm}\frac{(1+\xi\cos\theta)}{4\mathcal{B}}E_\xi(\Gamma_+^e+\Gamma_-^e) \times\big\{\kappa_{l,\xi}^a[\Gamma_\xi^e\Gamma_{\bar\xi}^a + (\Gamma_+^e+\Gamma_-^e)\Gamma_p^\xi] - \kappa_{l,\xi}^e(\Gamma_+^a\Gamma_-^a + \Gamma_+^a\Gamma_p^+ + \Gamma_-^a\Gamma_p^-)\big\}, \quad (15)$$

$$J_r = \sum_{\xi=\pm}\frac{(1-\xi\cos\theta)}{4\mathcal{B}}E_\xi(\Gamma_+^e+\Gamma_-^e) \times\big\{\kappa_{r,\xi}^a[\Gamma_\xi^e\Gamma_{\bar\xi}^a + (\Gamma_+^e+\Gamma_-^e)\Gamma_p^\xi] - \kappa_{r,\xi}^e(\Gamma_+^a\Gamma_-^a + \Gamma_+^a\Gamma_p^+ + \Gamma_-^a\Gamma_p^-)\big\}, \quad (16)$$

with $\bar\xi \equiv -\xi$. The current into the middle bath is

$$J_m = -(E_+-E_-)\frac{\Gamma_+^e+\Gamma_-^e}{\mathcal{B}}(\Gamma_+^a\Gamma_-^e\Gamma_p^+ - \Gamma_-^a\Gamma_+^e\Gamma_p^-), \quad (17)$$

where the coefficient is $\mathcal{B} = \sum_{\xi=\pm}(\Gamma_\xi^a + \Gamma_+^e + \Gamma_-^e)[\Gamma_\xi^e\Gamma_{\bar\xi}^a + (\Gamma_+^e+\Gamma_-^e)\Gamma_p^\xi]$, the combined rates are $\Gamma_+^{e(a)} = \frac{1}{2}(\kappa_{l,+}^{e(a)}\cos^2\frac{\theta}{2} + \kappa_{r,+}^{e(a)}\sin^2\frac{\theta}{2})$, $\Gamma_-^{e(a)} = \frac{1}{2}(\kappa_{l,-}^{e(a)}\sin^2\frac{\theta}{2} + \kappa_{r,-}^{e(a)}\cos^2\frac{\theta}{2})$, and $\Gamma_p^{+(-)} = \frac{\sin^2\theta}{2}\kappa_p^{e(a)}$, with the local rates $\kappa_{u,\pm}^e = \Lambda_u(E_\pm)n_u(E_\pm)$, $\kappa_{u,\pm}^a = \Lambda_u(E_\pm)[1+n_u(E_\pm)]$, $\kappa_p^e = \Lambda_m(E_+-E_-)n_m(E_+-E_-)$, and $\kappa_p^a = \Lambda_m(E_+-E_-)[1+n_m(E_+-E_-)]$.

We plot the currents [Eqs. (15)–(17)] in Fig. 2 to analyze the valid regime of α_m by comparing with the counterpart based on the PTRE. It is found that for J_l and J_r, the Redfield scheme is applicable even for the system–middle bath coupling strength $\alpha = 0.1$. While for J_m, the Redfield scheme becomes invalid as the system–middle bath coupling strength surpasses 0.01. This fact indicates that the influence of the phonons in the middle bath should be necessarily included to describe the transitions between $|\pm\rangle_\eta$ and $|0\rangle$, which may enhance the energy flow into the middle bath accordingly.

In the following, based on the consistent analysis of the heat currents (particular for J_m) we approximately classify the strength of the system–middle bath interaction into three regimes: (i) weak coupling regime $\alpha_m < 0.01$; (ii) moderate coupling regime $0.01 \le \alpha_m \le 2$; (iii) strong coupling regime $\alpha_m > 2$.

4. Results and discussion

Heat amplification and negative differential thermal conductance are considered as two crucial components of the quantum thermal transistor. Particularly for heat amplification, the schematic which is shown in Fig. 1(a) has the ability to significantly enhance the heat flow into the left or right terminal by a tiny modulation of the middle terminal temperature. Formally, the amplification factor is defined as[12]

$$\beta_u = \left|\partial J_u/\partial J_m\right|, \quad u = l, r. \tag{18}$$

Moreover, owning to the flux conservation of the three-level system $J_l + J_m + J_r = 0$, the amplification factors β_l and β_r are related by $\beta_l = \left|\beta_r + (-1)^\theta\right|$, with $\theta = 0$ when $\partial J_r/\partial J_m > 0$, and $\theta = 1$ when $\partial J_r/\partial J_m < 0$. The thermal transistor is properly functioning under the condition $\beta_{l(r)} > 1$. Currently, it is known that the heat amplification can be realized mainly via two mechanisms: (i) one is driven by NDTC within the two-terminal setup, where the heat current is suppressed with the increase of the temperature bias;[12,16] (ii) the other is driven by the inelastic transfer process without NDTC, which can be unraveled even in the linear response regime.[23]

4.1. Transistor effect

We first analyze the effect of the system-middle bath interaction on the heat amplification of the nonequilibrium three-level system, shown in Fig. 4. It is found that the giant amplification factor appears in the moderate and strong system-middle bath coupling regimes both for the low and high temperature biases between the left and right thermal baths. Moreover, the finite amplification factor can be observed at the high temperature bias with weak system-middle bath coupling strength. Hence, we mainly investigate the behavior and the underlying mechanism of the heat amplification at the high temperature bias.

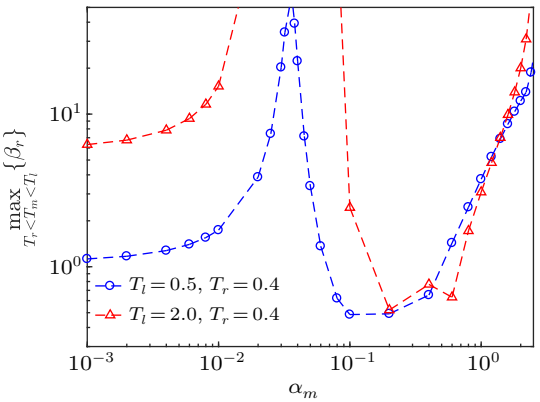

Fig. 4. Heat amplification factor as a function of system–middle bath coupling strength α_m in low ($T_l = 0.5$, $T_r = 0.4$) and high ($T_l = 2$, $T_r = 0.4$) temperature bias regimes, with $\max_{T_r<T_m<T_l}\{\beta_r\}$ the maximal value of β_r by tuning the temperature of the middle bath T_m between T_r and T_l. The other parameters are given by $\varepsilon_l = 1.0$, $\varepsilon_r = 0.6$, $\Delta = 0.6$, $\gamma = 0.0002$, and $\omega_c = 10$.

4.1.1. Heat amplification at strong coupling

We first investigate the influence of the strong system–middle bath interaction on the heat amplification by tuning the temperature T_m of the middle bath. As shown in Fig. 5(a), the amplification factor is monotonically enhanced when the coupling strength increases from the moderate coupling regime (e.g., $\alpha_m = 0.5$). When the interaction strength enters the strong coupling regime ($\alpha_m = 2$), the amplification factor becomes large but finite in the low temperature regime of T_m (see Appendix B3 for brief analysis), whereas it is strongly suppressed as T_m reaches $T_m = T_l = 2$. Interestingly, as α_m is further strengthened (e.g., up to 4), a giant heat amplification appears with a divergent point, which results form the turnover behavior of J_m shown in the inset of Fig. 5(b). Moreover, the heat currents into the left and right thermal baths in Fig. 5(b) corresponding to $\alpha_m = 4$ are much larger than J_m, which ensures the validity of the heat amplification in the strong coupling regime.

Next, we give a comprehensive picture of the amplification factor by modulating the temperature T_m and coupling strength α_m in Fig. 5(c). It is found that the divergent behavior of the heat amplification is generally robust in the strong coupling regime ($\alpha_m \gtrsim 2.8$). In summary, we conclude that the giant heat amplification feature favors the strong system–middle bath interaction.

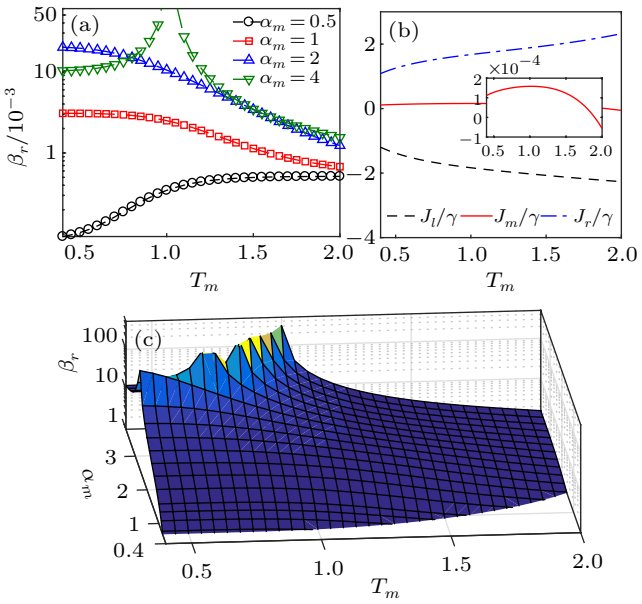

Fig. 5. (a) Heat amplification factor β_r as a function of the middle bath temperature T_m with various system–middle bath coupling strength α_m; (b) three steady state heat currents J_u/γ $(u = l, m, r)$ as a function of T_m with the coupling strength $\alpha_m = 4$, and the inset is the zoom in view of J_m/γ; (c) the 3D view of the heat amplification factor β_r by tuning T_m and α_m. The other parameters are given by $\varepsilon_l = 1.0$, $\varepsilon_r = 0.6$, $\Delta = 0.6$, $\gamma = 0.0002$, $\omega_c = 10$, $T_l = 2$, and $T_r = 0.4$.

4.1.2. Mechanism of the giant heat amplification

We devote this subsection to exploring the underlying mechanism of the giant heat amplification β_r at strong system–middle bath coupling regime (e.g., $\alpha_m = 4$) based on the analytical expressions of heat currents in Eqs. (11) and (12). The limiting condition of large energy gap ($-E_r \gg 1$) and low temperature of the right bath results in the vanishing phonon excitation $n_r(\omega \approx -E_r) \approx 0$. Thus, the factor G_r^- shows negligible

contribution to the transition between the states $|r\rangle$ and $|0\rangle$, which is shown in Fig. 6(a). Moreover, the large energy gap $(-E_{l(r)} \gg 1)$ also generally leads to $G^{+}_{l(r)} \gg G^{-}_{l(r)}$. Hence, the heat current J_r is simplified as

$$J_{r,\mathrm{NIBA}} \approx \frac{1}{\mathcal{A}} G^{-}_{l} G^{-}_{m} G^{+}_{r} \langle\omega\rangle_{r,+}, \tag{19}$$

with the coefficient reduced to $\mathcal{A} \approx (G^{+}_{m} + G^{-}_{m})(G^{+}_{l} + G^{+}_{r})$. $J_{r,\mathrm{NIBA}}$ is determined by the globally cyclic transition $|0\rangle \to |l\rangle \to |r\rangle \to |0\rangle$, which is characterized by the cooperative rate $\frac{1}{\mathcal{A}} G^{-}_{l} G^{-}_{m} G^{+}_{r}$. Moreover, it should be noted that though G^{+}_{m} is much larger than G^{-}_{m}, the ratio $G^{-}_{m}/G^{+}_{m} = \exp[-(\varepsilon_l - \varepsilon_r)/(k_{\mathrm{B}} T_m)]$ shows monotonic increase as a function of T_m [see dashed lines with circles and up-triangles in Fig. 6(a)]. Then, by tuning up the temperature T_m from $T_r = 0.4$, the increase of G^{-}_{m}/G^{+}_{m} dominates the monotonic enhancement of $J_{r,\mathrm{NIBA}}$, as the rates $G^{\pm}_{l}$, G^{+}_{r} and energy $\langle\omega\rangle_{r,+}$ are nearly constant as shown in Figs. 6(a) and 6(b).

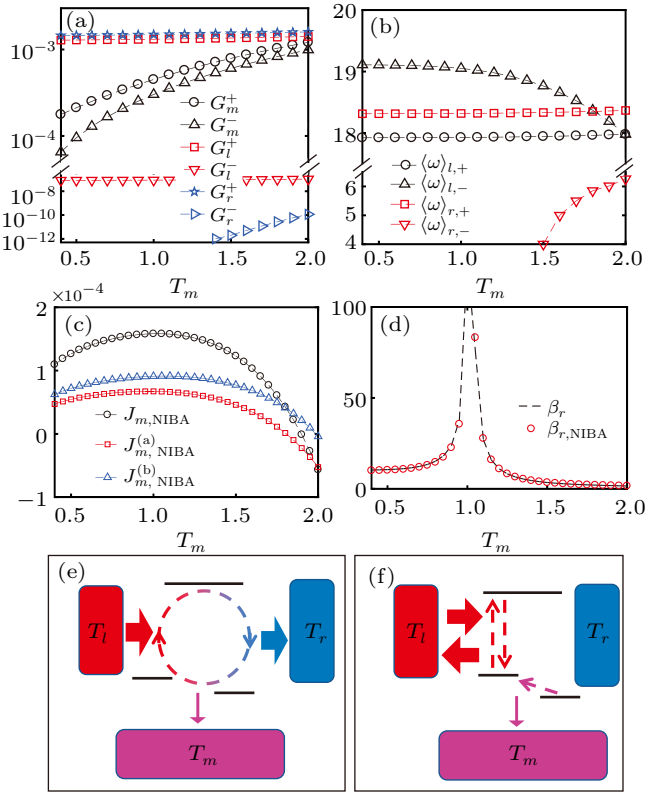

Fig. 6. Steady state behaviors as a function of the middle bath temperature T_m within the nonequilibrium NIBA at strong coupling ($\alpha_m = 4$): (a) transition rates $G^{\pm}_{u}$ $(u = l, m, r)$ in Eqs. (13a)–(13c), and (b) average energy quanta $\langle\omega\rangle_{u,\pm}$ $(u = l, r)$ in Eqs. (14a) and (14b); (c) heat current $J_{m,\mathrm{NIBA}}$ and its main components in Eqs. (20a) and(20b), and (d) comparison of the approximate amplification factor $\beta_{r,\mathrm{NIBA}}$ with β_r. (e) and (f) Schematic illustrations of flow components $J^{(a)}_{m,\mathrm{NIBA}}$ and $J^{(b)}_{m,\mathrm{NIBA}}$. The other parameters are the same as those in Fig. 5.

However, the current $J_{m,\mathrm{NIBA}}$ is no longer a monotonic function of T_m, which owns a maximum $T_m \approx 1$ as illustrated in Fig. 6(c). The existence of a turnover point of T_m is crucial to the giant heat amplification, so it worths a careful study on $J_{m,\mathrm{NIBA}}$. As G^{-}_{r} is negligible, $J_{m,\mathrm{NIBA}}$ can be approximated as the sum of two terms $J_{m,\mathrm{NIBA}} \approx J^{(a)}_{m,\mathrm{NIBA}} + J^{(b)}_{m,\mathrm{NIBA}}$, with components

$$J^{(a)}_{m,\mathrm{NIBA}} = \frac{1}{\mathcal{A}} G^{-}_{m} G^{-}_{l} G^{+}_{r} (\langle\omega\rangle_{l,-} - \langle\omega\rangle_{r,+}), \tag{20a}$$

$$J^{(b)}_{m,\mathrm{NIBA}} = \frac{1}{\mathcal{A}} G^{-}_{m} G^{-}_{l} G^{+}_{l} (\langle\omega\rangle_{l,-} - \langle\omega\rangle_{l,+}). \tag{20b}$$

The approximate factor $\beta_{r,\mathrm{NIBA}} = \left|\partial J_{r,\mathrm{NIBA}}/\partial (J^{(a)}_{m,\mathrm{NIBA}} + J^{(b)}_{m,\mathrm{NIBA}})\right|$ is agreeable with the counterpart obtained by the PRTE, shown in Fig. 6(d). Specifically, $J^{(a)}_{m,\mathrm{NIBA}}$ describes a globally cyclic current with the loop rate $G^{-}_{m} G^{-}_{l} G^{+}_{r}/\mathcal{A}$ to extract energy $\langle\omega\rangle_{l,-}$ out of the l-th bath and input $\langle\omega\rangle_{r,+}$ into the r-th bath, the resultant energy difference $(\langle\omega\rangle_{l,-} - \langle\omega\rangle_{r,+})$ is absorbed by the middle bath. While $J^{(b)}_{m,\mathrm{NIBA}}$ is only associated with the local transition process between states $|l\rangle$ and $|0\rangle$, and each transition pumps energy $(\langle\omega\rangle_{l,-} - \langle\omega\rangle_{l,+})$ out of the left bath into the middle bath. These two currents are schematically illustrated in Figs. 6(e) and 6(f), respectively.

For both $J^{(a)}_{m,\mathrm{NIBA}}$ and $J^{(b)}_{m,\mathrm{NIBA}}$, only the factors G^{-}_{m}/G^{+}_{m} and $\langle\omega\rangle_{l,-}$ are obvious dependent on T_m, whereas all the other factors can be approximately treated constant. In the low temperature regime of T_m, the increase behavior of $J_{m,\mathrm{NIBA}}$ is due to the increase of G^{-}_{m}/G^{+}_{m}. However, as the temperature T_m passing the turnover point, the monotonically decrease of $\langle\omega\rangle_{l,-}$ leads to the suppression of $J_{m,\mathrm{NIBA}}$ [see Fig. 6(b)]. Therefore, the turnover behavior of J_m mainly results in the giant heat amplification factor.

4.1.3. Heat amplification at weak and moderate couplings

We investigate heat amplification at weak system–middle bath coupling in Fig. 7(a). It is found that in the weak coupling regime (e.g., $\alpha_m = 0.001$, the dashed black line with circles), the three-level system shows amplifying ability with finite amplification factor ($\beta_r \approx 6$) in the low temperature regime $T_m \in [0.4, 1.1]$. This result is consistent with the counterpart from the Redfield equation (dashed-dotted line). This clearly demonstrates the existence of the amplification effect in absence of the NDTC. Then, we analytically estimate the amplification factor. It is found that the phonon from the middle bath is not involved in the transition process between $|\pm\rangle_{\eta}$ and $|0\rangle$, resulting in $\mathrm{Re}[\kappa_{u,+}(E_{\pm})] \approx \kappa^{e}_{u,\pm}/2$ and $\mathrm{Re}[\kappa_{u,-}(E_{\pm})] \approx \kappa^{a}_{u,\pm}/2$, with $\kappa^{e}_{u,\pm} = \Lambda_u(E_{\pm}) n_u(E_{\pm})$ and $\kappa^{a}_{u,\pm} = \Lambda_u(E_{\pm})[1 + n_u(E_{\pm})]$. Then, the current into the middle bath is shown as $J_m \propto (\Gamma^{a}_{+}\Gamma^{e}_{-}\Gamma^{+}_{p} - \Gamma^{a}_{-}\Gamma^{e}_{+}\Gamma^{-}_{p})$ [see the full expression in Eq. (17)], which is contributed by two cyclic flows, demonstrating the inelastic transport process. Moreover, considering the limiting case $E_{+} \gg E_{-}$, $\Gamma^{\pm}_{p} \gg \Gamma^{a(e)}_{-}$ and $\Gamma^{a(e)}_{+} \gg \Gamma^{a(e)}_{-}$, the current into the right bath with high temperature bias ($T_l \gg T_r$) is generally dominated by the component $J_r \propto (\kappa^{a}_{r,+}\Gamma^{e}_{+} - \kappa^{e}_{r,+}\Gamma^{a}_{+})\Gamma^{+}_{p}$. Both J_m and J_r are shown to be strongly affected by $G^{\pm}_{p}$, which implies the inelastic exchange process. It is interacting to find the linear relationship of currents $\partial J_r/\partial T_m = \beta_r \partial J_m/\partial T_m$, where the amplification factor

is approximately expressed as [see Eq. (C16) in Appendix C]

$$\beta_r \approx \frac{\sin^2\theta}{16}\left|\frac{\kappa^e_{l,+}\kappa^a_{r,+}-\kappa^a_{l,+}\kappa^e_{r,+}}{\Gamma^a_-(\Gamma^a_++\Gamma^e_+)+\Gamma^a_+\Gamma^e_-}\right|, \tag{21}$$

which is irrelevant to T_m and α_m. While in the low temperature bias limit ($T_l \approx T_r$), due to $\kappa^{a(e)}_{l,\pm}\approx\kappa^{a(e)}_{r,\pm}$, the current into the right bath is determined by the current component $J_r\propto(\kappa^a_{r,+}\Gamma^e_-\Gamma^+_p-\kappa^e_{r,+}\Gamma^a_-\Gamma^-_p)$. Then, the amplification factor is approximated as $\beta_r\approx(1-\cos\theta)/2$, which demonstrates that the amplification effect becomes weak. This is qualitatively consistent with the result shown in Fig. 4 with weak system–middle bath coupling strength (e.g., $\beta_r\approx1$ with $\alpha_m=0.001$).

If we increase the coupling strength α_m up to the moderate regime (e.g., $\alpha_m=0.02$), the giant amplification factor appears in the comparatively low temperature regime [dashed line with up-triangle in Fig. 7(a)], which is due to the turnover behavior of J_m in Fig. 7(b). Such feature results from NDTC, which will be addressed in the following subsection. It should be emphasized that the heat amplification is purely explored by the PTRE, which however cannot be explained with the Redfield equation.

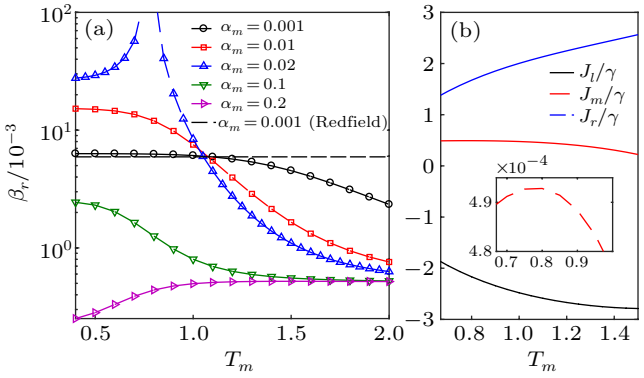

Fig. 7. (a) Heat amplification factor β_r with various coupling strengthes α_m, and (b) steady state heat currents with $\alpha_m=0.02$ as a function of T_m, the inset is the zoom-in view of J_m/γ. The other parameters are the same as those in Fig. 5.

4.2. Negative differential thermal conductance

To better understand the amplification effect in Fig. 7, we investigate the steady state heat current within the two-terminal setup (the l-th and m-th thermal baths), schematically shown in Fig. 8(a). We stress that the phonon in the middle bath should be necessarily included to induce NDTC. Specifically, we keep one phonon transfer process for the rate $\gamma_{x(y)}(\omega)$. While for rates $\kappa_{u,\pm}$, we first consider the zeroth order as $\kappa^{(0)}_{u,+}(E_\pm)=\eta_u^2\kappa^e_{u,\pm}/2$ and $\kappa^{(0)}_{u,-}(E_\pm)=\eta_u^2\kappa^a_{u,\pm}/2$. Then, the zeroth order heat current $J^{(0)}$ obtained from the PTRE shows monotonic enhancement by increasing the temperature bias T_l-T_m in Fig. 8(b), which demonstrates no NDTC signature. Next, we include the first order corrections to the transition rates as

$$\kappa^{(1)}_{u,+}(E_\pm) = \kappa^{(0)}_{u,+}(E_\pm)+\int_{-\infty}^{\infty}\frac{\mathrm{d}\omega_1}{4\pi}\Lambda_u(\omega_1)n_u(\omega_1) \times\mathrm{Re}\left[C^{(1)}_u(\omega_1-E_\pm)\right], \tag{22a}$$

$$\kappa^{(1)}_{u,-}(E_\pm) = \kappa^{(0)}_{u,-}(E_\pm)+\int_{-\infty}^{\infty}\frac{\mathrm{d}\omega_1}{4\pi}\Lambda_u(\omega_1)[1+n_u(\omega_1)] \times\mathrm{Re}\left[C^{(1)}_u(-\omega_1+E_\pm)\right], \tag{22b}$$

with the single phonon correlation function $C^{(1)}_u(\pm\omega_1\mp E_\pm)=\frac{\eta_u^2}{4}\int_0^\infty \mathrm{d}\tau\,\mathrm{e}^{\mathrm{i}(\pm\omega_1\mp E_\pm)\tau}\phi_m(\tau)$. The heat current $J^{(1)}_{\text{polaron}}$ up to the first order correction shows interesting NDTC feature, which is almost identical with the exact numerical solution from the PTRE J. Therefore, we conclude that the middle bath phonon induced transition between $|0\rangle$ and $|\pm\rangle_\eta$ is crucial to the appearance of NDTC, as shown in Fig. 8(a), which cannot be found from the standard Redfield scheme.

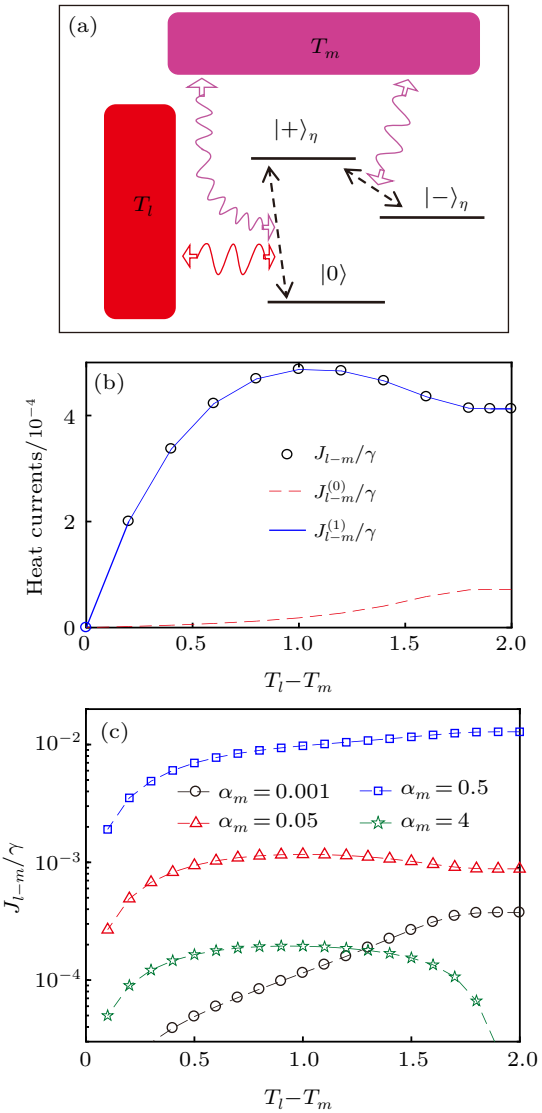

Fig. 8. (a) Schematic illustration of quantum thermal transport in the three-level system ($|\pm\rangle_\eta$ and $|0\rangle$) contacting with the l-th and m-th thermal baths; (b) steady state heat currents by modulating the temperature bias T_l-T_m, which have different order approximations with $\alpha_m=0.02$; (c) steady state heat currents by tuning the temperature bias T_l-T_m with various system–middle bath coupling strengthes. The temperature of the left thermal bath is $T_l=2$, and the other parameters are the same as those in Fig. 5.

Moreover, we investigate the effect of the system–middle bath coupling strength on the steady state heat currents by modulating the temperature bias T_l-T_m, as shown in Fig. 8(c). It is found that besides the emergence of NDTC with mod-

erate interaction strength (e.g., $\alpha_m = 0.05$), the nonmonotonic behavior of the current is also clearly seen at strong system–middle bath coupling $\alpha_m = 4$. With certain approximation, such NDTC can be explained within the nonequilibrium NIBA, by which the current is simplified to

$$J_{l-m}=\frac{1}{\mathcal{A}'}G_m^- G_l^+ G_l^- (\langle\omega\rangle_{l,-}-\langle\omega\rangle_{l,+}), \tag{23}$$

with $\mathcal{A}' = (G_m^+ + G_m^-)G_l^+ + G_m^- G_l^-$. It should be noted that $G_{l(m)}^{\pm}$ and $\langle\omega\rangle_{l,\pm}$ in this two-terminal case have the identical expression as shown in Eqs. (13a)–(13c) and (14a)–(14b) within the three-terminal setup, respectively. Considering the dramatic suppression of the transition rate G_m^- with large temperature bias $T_l - T_m$, i.e., low temperature regime of T_m in Fig. 6(a), the transition from $|r\rangle$ to $|l\rangle$ is strongly blocked, which dramatically suppresses the flux rate in J_{l-m}. It finally leads to NDTC.

5. Conclusion

To summarize, we study the steady state heat currents in the nonequilibrium three-level system interacting with three individual thermal baths. We apply the PTRE combined with FCS to investigate the system density matrix and the resultant heat currents. In the weak and strong system–middle bath coupling limits, we obtain the analytical expression of heat currents with the Redfield scheme and nonequilibrium NIBA approach, which are consistent with the counterpart of the PTRE. This extends the application of the PTRE to the nonequilibrium three-level models from the previous nonequilibrium (coupled) spin-boson model.

We also study the thermal transistor effect by tuning the system–middle bath coupling strength from weak to strong coupling regimes. We first explore the giant heat amplification factor with strong coupling. It is found that the globally cyclic current component and middle bath mediated local current component are crucial to exhibit the turnover behavior of the current into the middle bath. The joint cooperation between the rates ratio G_m^-/G_m^+ assisted by the middle thermal bath and energy $\langle\omega\rangle_{l,-}$ mainly results in such heat amplification feature. Next, we investigate heat amplification at weak and moderate system–middle bath couplings. In the weak coupling regime, the finite heat amplification in absence of NDTC is discovered, and analytically estimated by the Redfield scheme. It is mainly attributed to the inelastic transport process. While in the moderate coupling regime, it is interesting to find another giant amplification signature, which is mainly contributed by the middle bath assisted thermal transport between states $|\pm\rangle_\eta$ and $|0\rangle$. Therefore, we clearly observe two different types of the heat amplification effect by tuning the system–middle bath interaction in a wide regime, and explore the corresponding microscopic mechanisms, which are the answers for the questions in the introduction. Moreover, we also analyze the corresponding NDTC effect with the two-terminal setup. It should be noted that such giant amplification and NDTC behaviors cannot be explained by the Redfield scheme, which clearly demonstrates the wide application of the PTRE.

We hope the analysis of the heat amplification and negative differential thermal conductance may provide some theoretical insight in design of the quantum thermal transistor.

Appendix A: FCS of heat currents in three-level quantum system

Based on the full counting statistics, it is known that the steady state current into the u-th bath J_u is expressed as[33,49] $J_u = \frac{\partial}{\partial(\mathrm{i}\chi_u)}[\lim_{\tau\to\infty}\frac{1}{\tau}\ln\mathcal{Z}(\chi_u,\tau)]\Big|_{\chi_u=0}$, where the generating function is $\mathcal{Z}(\chi_u,\tau) = \mathrm{Tr}[\hat{\rho}_{\chi_u}(\tau)]$ and the counting parameter dependent system density matrix is $\hat{\rho}_{\chi_u}(\tau) = \mathrm{e}^{-\mathrm{i}\tau\hat{H}_{-\chi_u}}\hat{\rho}_{\mathrm{tot}}(0)\,\mathrm{e}^{\mathrm{i}\tau\hat{H}_{\chi_u}}$, with the modified Hamiltonian $\hat{H}_{\chi_u} = \mathrm{e}^{\mathrm{i}\chi_u\hat{H}_b^u/2}\hat{H}\,\mathrm{e}^{-\mathrm{i}\chi_u\hat{H}_b^u/2}$ and $\hat{\rho}_{\mathrm{tot}}(0)$ the initial density matrix operator of the whole system. Specifically, the time evolution of $\hat{\rho}_{\chi_u}(\tau)$ can be equivalently written in the differential form of the quantum Liouvillian equation with an effective Hamiltonian including the counting parameters $\hat{H}_{\{\chi\}} = \hat{H}_s + \sum_{u=l,m,r}\hat{H}_b^u + \hat{V}_m + \sum_{u=l,r}\hat{V}_u(\chi_u)$, where $\{\chi\} = (\chi_l,\chi_r)$ is a set of parameters counting both the heat flows from the left and right baths. The modified system–bath interactions are

$$\hat{V}_u(\chi_u) = (\hat{S}_u^\dagger + \hat{S}_u)\sum_k\left(g_{k,u}\,\mathrm{e}^{\mathrm{i}\omega_k\chi_u/2}\hat{b}_{k,u}^\dagger + \mathrm{H.c.}\right),\quad u = l,r. \tag{A1}$$

By applying the unitary transformation $\hat{H}' = \hat{U}^\dagger\hat{H}\hat{U}$ with $\hat{U} = \exp[\mathrm{i}\hat{B}(|l\rangle\langle l| - |r\rangle\langle r|)]$, the transformed Hamiltonian becomes $\hat{H}_s' + \sum_{u=l,m,r}\hat{H}_b^u + \hat{V}_m + \sum_{u=l,r}\hat{V}_u(\chi_u)$. In particular, $\hat{V}_u(\chi_u)$ is transformed to

$$\hat{V}_u'(\chi_u) = \left(\mathrm{e}^{-\mathrm{i}\hat{B}_u}\hat{S}_u^\dagger + \mathrm{e}^{\mathrm{i}\hat{B}_u}\hat{S}_u\right)\sum_k(g_{k,u}\,\mathrm{e}^{\mathrm{i}\omega_k\chi_u/2}\hat{b}_{k,u}^\dagger + \mathrm{H.c.}). \tag{A2}$$

With the same approach introduced in Subsection 2.2, we obtain the PTRE of system density operator $\hat{\rho}_{\{\chi\}}$, which can be marked by the counting parameters as

$$\frac{\mathrm{d}}{\mathrm{d}t}\hat{\rho}_{\{\chi\}} = -\mathrm{i}\left[\hat{H}_s', \hat{\rho}_{\{\chi\}}\right] + \mathcal{L}_m\left[\hat{\rho}_{\{\chi\}}\right] + \sum_{u=l,r}\mathcal{L}_{\chi_u}^u\left[\hat{\rho}_{\{\chi\}}\right]. \tag{A3}$$

Here, the generalized dissipator is

$$\begin{aligned}\mathcal{L}_{\chi_u}^u[\hat{\rho}_{\{\chi\}}] = \sum_{\omega,\omega'}\{&\kappa_{u,+}(\omega',\chi_u)\hat{Q}_u^\dagger(\omega')\hat{\rho}_{\{\chi\}}\hat{Q}_u(\omega)\\ &+\kappa_{u,-}(\omega',\chi_u)\hat{Q}_u(\omega')\hat{\rho}_{\{\chi\}}\hat{Q}_u^\dagger(\omega)\\ &+\kappa_{u,+}^*(\omega',-\chi_u)\hat{Q}_u^\dagger(\omega)\hat{\rho}_{\{\chi\}}\hat{Q}_u(\omega')\\ &+\kappa_{u,-}^*(\omega',-\chi_u)\hat{Q}_u(\omega)\hat{\rho}_{\{\chi\}}\hat{Q}_u^\dagger(\omega')\\ &-\left[\kappa_{u,+}(\omega')\hat{Q}_u(\omega)\hat{Q}_u^\dagger(\omega')\hat{\rho}_{\{\chi\}}\right.\\ &\left.+\kappa_{u,-}(\omega')\hat{Q}_u^\dagger(\omega)\hat{Q}_u(\omega')\hat{\rho}_{\{\chi\}} + \mathrm{H.c.}\right]\},\end{aligned} \tag{A4}$$

with the generalized dissipation rates

$$\kappa_{u,+}(\omega',\chi_u) = \int_{-\infty}^{\infty}\frac{\mathrm{d}\omega_1}{4\pi}\Lambda(\omega_1)n_u(\omega_1)\,\mathrm{e}^{-\mathrm{i}\omega_1\chi_u}C_u(\omega_1-\omega'), \tag{A5a}$$

$$\kappa_{u,-}(\omega',\chi_u)=\int_{-\infty}^{\infty}\frac{\mathrm{d}\omega_1}{4\pi}\Lambda(\omega_1)[1+n_u(\omega_1)]\,\mathrm{e}^{\mathrm{i}\omega_1\chi_u}C_u(-\omega_1+\omega'). \tag{A5b}$$

In absence of the counting parameters ($\chi_l=0,\chi_r=0$), the density operator $\hat{\rho}_{\{\chi\}}$, the dissipator $\mathcal{L}^u_{\chi_u}[\hat{\rho}_{\{\chi\}}]$, and dissipation rates $\kappa_{u,\pm}(\omega',\chi_u)$ are reduced to the original $\hat{\rho}_s$, $\mathcal{L}_u[\hat{\rho}_s]$, and $\kappa_{u,\pm}(\omega')$ defined in Subsection 2.2, respectively.

Furthermore, we re-express the dynamical equation of Eq. (A3) as $\frac{\mathrm{d}}{\mathrm{d}t}|\boldsymbol{P}_{\{\chi\}}\rangle\rangle=\mathbb{L}_{\{\chi\}}|\boldsymbol{P}_{\{\chi\}}\rangle\rangle$, where $|\boldsymbol{P}_{\{\chi\}}\rangle\rangle=[\rho^{\{\chi\}}_{++},\rho^{\{\chi\}}_{--},\rho^{\{\chi\}}_{00},\rho^{\{\chi\}}_{+-},\rho^{\{\chi\}}_{-+}]^{\mathrm{T}}$ is the vector form of the reduced density matrix, with $\rho^{\{\chi\}}_{ij}=\langle i|\hat{\rho}_{\{\chi\}}|j\rangle$ $(i,j=0,\pm)$, and $\mathbb{L}_{\{\chi\}}$ is the super-operator defined according to Eq. (A3). Therefore, the heat currents flowing into the left and right thermal baths can be expressed as[34]

$$J_u=\langle\langle\boldsymbol{I}|\frac{\partial\mathbb{L}_{\{\chi\}}}{\partial(i\chi_u)}\bigg|_{\chi=0}|\boldsymbol{P}\rangle\rangle, \tag{A6}$$

with the steady state $|\boldsymbol{P}\rangle\rangle=|\boldsymbol{P}_{\{\chi\}}\rangle\rangle$ and $\langle\langle\boldsymbol{I}|=[1,1,1,0,0]$ and $u=l,r$. The steady state current into the middle bath is obtained by the energy conservation condition as $J_m=-J_l-J_r$. It should be noted that though not shown here, the energy conservation is verified by counting the energy flows into the three baths individually.

Appendix B: Nonequilibrium NIBA scheme

B1. Steady state heat currents

In the strong system–middle bath coupling regime, the modified Hamiltonian in Eq. (4) is reduced to $\hat{H}'_{s,\mathrm{NIBA}}=\bar{\varepsilon}\hat{N}+\delta\varepsilon\hat{\sigma}_z$, and the system–middle bath interaction in Eq. (5a) becomes $V'_{m,\mathrm{NIBA}}=\mathrm{e}^{\mathrm{i}\hat{B}}\hat{\sigma}_-+\mathrm{H.c.}$ Combined with full counting statistics, the dynamical equation of populations in Eq. (A3) is specified as

$$\begin{aligned}\frac{\mathrm{d}P^{\chi}_l}{\mathrm{d}t}=&-G_m(2\delta\varepsilon)P^{\chi}_l+G^{\chi_m}_m(-2\delta\varepsilon)P^{\chi}_r-G_{l,-}(E_l)P^{\chi}_l\\&+G^{\chi_l,\chi_m}_{l,+}(E_l)P^{\chi}_m,\end{aligned} \tag{B1a}$$

$$\begin{aligned}\frac{\mathrm{d}P^{\chi}_r}{\mathrm{d}t}=&-G_m(-2\delta\varepsilon)P^{\chi}_r+G^{\chi_m}_m(2\delta\varepsilon)P^{\chi}_l-G_{r,-}(E_r)P^{\chi}_r\\&+G^{\chi_r,\chi_m}_{r,+}(E_r)P^{\chi}_m,\end{aligned} \tag{B1b}$$

$$\frac{\mathrm{d}P^{\chi}_m}{\mathrm{d}t}=-\sum_{u=l,r}G_{u,+}(E_u)P_m+\sum_{u=l,r}G^{\chi_u,\chi_m}_{u,-}(E_u)P^{\chi}_u, \tag{B1c}$$

where the transition rates are

$$G^{\chi_m}_m(\omega)=\mathrm{e}^{\mathrm{i}\omega\chi_m}\int_{-\infty}^{\infty}\mathrm{d}\tau\,\mathrm{e}^{\mathrm{i}\omega\tau}\eta^2\,\mathrm{e}^{\phi_m(\tau)}, \tag{B2a}$$

$$\begin{aligned}G^{\chi_u,\chi_m}_{u,+}=&\frac{1}{4\pi}\int_{-\infty}^{\infty}\mathrm{d}\omega_1\Lambda_u(\omega_1)[1+n_u(\omega_1)]\,\mathrm{e}^{\mathrm{i}\omega_1\chi_u}\,\mathrm{e}^{-\mathrm{i}(\omega_1+E_u)\chi_m}\\&\times[C_u(-\omega_1-E_u)+\mathrm{H.c.}],\end{aligned} \tag{B2b}$$

$$\begin{aligned}G^{\chi_u,\chi_m}_{u,-}=&\frac{1}{4\pi}\int_{-\infty}^{\infty}\mathrm{d}\omega_1\Lambda_u(\omega_1)n_u(\omega_1)\,\mathrm{e}^{-\mathrm{i}\omega_1\chi_u}\,\mathrm{e}^{\mathrm{i}(E_u+\omega_1)\chi_m}\\&\times[C_u(E_u+\omega_1)+\mathrm{H.c.}].\end{aligned} \tag{B2c}$$

In absence of counting parameters, the steady state populations are obtained as

$$P_m=\frac{1}{\mathcal{A}}(G^+_mG^-_r+G^-_mG^-_l+G^-_lG^-_r), \tag{B3a}$$

$$P_l=\frac{1}{\mathcal{A}}(G^-_mG^+_l+G^-_mG^+_r+G^+_lG^-_r), \tag{B3b}$$

$$P_r=\frac{1}{\mathcal{A}}(G^+_mG^+_l+G^+_mG^+_r+G^-_lG^+_r), \tag{B3c}$$

with the coefficient $\mathcal{A}=(G^+_m+G^-_m)(G^+_l+G^+_r)+G^+_mG^-_r+G^-_mG^-_l+G^-_lG^+_r+G^-_r(G^+_l+G^-_l)$. And the currents into the left and right baths are given by

$$J_u=G^+_u\langle\omega\rangle_{u,+}P_m-G^-_u\langle\omega\rangle_{u,-}P_u,\quad(u=l,r), \tag{B4}$$

with the energy

$$\begin{aligned}\langle\omega\rangle_{u,+}=&\frac{1}{4\pi G^+_u}\int\mathrm{d}\omega_1\omega_1\Lambda_u(\omega_1)[1+n_u(\omega_1)]\\&\times[C_u(-E_u-\omega_1)+\mathrm{H.c.}],\end{aligned} \tag{B5a}$$

$$\langle\omega\rangle_{u,-}=\frac{1}{4\pi G^-_u}\int\mathrm{d}\omega_1\omega_1\Lambda_u(\omega_1)n_u(\omega_1)[C_u(\omega_1+E_u)+\mathrm{H.c.}], \tag{B5b}$$

and $E_u=\varepsilon_u-\sum_k|g_{k,m}|^2/\omega_k$. The current into the middle bath based on the full counting statistics is given by

$$\begin{aligned}J_m=&-\frac{1}{\mathcal{A}}\big[G^+_mG^+_lG^-_r(\langle\omega\rangle_{l,+}-\langle\omega\rangle_{r,-})\\&+G^-_mG^-_lG^+_r(\langle\omega\rangle_{r,+}-\langle\omega\rangle_{l,-})\big]\\&-\frac{1}{\mathcal{A}}\big[(G^-_m+G^-_r)G^+_lG^-_l(\langle\omega\rangle_{l,+}-\langle\omega\rangle_{l,-})\\&+(G^+_m+G^-_l)G^+_rG^-_r(\langle\omega\rangle_{r,+}-\langle\omega\rangle_{r,-})\big].\end{aligned} \tag{B6}$$

B2. Behaviors of $G^{\pm}_u$ and $\langle\omega\rangle_{u,\pm}$ at strong system–middle bath coupling

We analyze the effect of the middle bath on the rates $G^{\pm}_u$ $(u=l,r)$ in Eqs. (13b) and (13c) and energy $\langle\omega\rangle_{u,\pm}$ in Eqs. (14a) and (14b) with strong system–middle bath interaction, where the renormalization energy becomes $(-E_u)\gg1$, with $E_u=(\varepsilon_u-\sum_k|g_{k,m}|^2/\omega_k)$. In particular for the rate G^-_r, the correlation function $C_r(\omega_1+E_u)$ makes the energy around $\omega_1\approx(-E_u)$ dominates the energy exchange process. Moreover, the cooperation of the large energy gap $(-E_u)$ and low temperature of the right bath (T_r) leads to the negligible boson excitation from the right bath [i.e., $n_r(-E_u)\approx0$]. Hence, G^-_r shows negligible contribution to the nonequilibrium energy transfer in the three-level system. Accordingly, the heat currents are simplified as

$$\begin{aligned}J_{l,\mathrm{NIBA}}=&\frac{1}{\mathcal{A}}[-G^-_lG^-_mG^+_r\langle\omega\rangle_{l,-}\\&+G^-_mG^-_lG^+_l(\langle\omega\rangle_{l,+}-\langle\omega\rangle_{l,-})],\end{aligned} \tag{B7a}$$

$$\begin{aligned}J_{m,\mathrm{NIBA}}=&\frac{1}{\mathcal{A}}[G^-_lG^-_mG^+_r(\langle\omega\rangle_{l,-}-\langle\omega\rangle_{r,+})\\&-G^-_mG^-_lG^+_l(\langle\omega\rangle_{l,+}-\langle\omega\rangle_{l,-})],\end{aligned} \tag{B7b}$$

$$J_{r,\mathrm{NIBA}}=\frac{1}{\mathcal{A}}G^-_lG^-_mG^+_r\langle\omega\rangle_{r,+}, \tag{B7c}$$

with $\mathcal{A}=(G^+_m+G^-_m)(G^+_l+G^+_r)$. However, it should be noted that though G^-_l is much smaller than $G^+_{l(r)}$ as shown in

Figs. B1(a)–B1(c), it can not be naively ignored. The main reason is that $J_{r,\mathrm{NIBA}}$ is contributed by the cyclic flux (the corresponding cycle is $|0\rangle\to|l\rangle\to|r\rangle\to|0\rangle$), which is assisted by the rate G_l^-.

Then, we study the effect of the middle thermal bath on the rates $G_{l(r)}^+$ and G_l^- in Figs. B1(a)–B1(c). It is found that by increasing the temperature T_m both rates show monotonic enhancement. This clearly demonstrates that the joint energy exchange process from the left (right) bath and the middle bath is crucial to characterize these transition rates, which can not be described with the zeroth order approximation

$$G_u^{+,(0)} \approx \frac{\eta_u^2}{2}\Lambda_u(-E_u)[1+n_u(-E_u)], \tag{B8a}$$

$$G_l^{-,(0)} \approx \frac{\eta_l^2}{2}\Lambda_u(-E_l)n_l(-E_l). \tag{B8b}$$

Moreover, the system–left (right) bath interaction is rather weak. Hence, one boson contribution of the middle bath can approximately quantify the transition rates. It results in the first order correction as

$$\begin{aligned} G_u^{+,(1)} \approx& \frac{\eta_u^2}{2}\Lambda_u(-E_u)[1+n_u(-E_u)] \\ &+ \frac{\eta_u^2}{8\pi}\int_{-\infty}^{\infty} \mathrm{d}\,\omega_1 \frac{\Lambda_u(\omega_1)\Lambda_m(-E_u-\omega_1)}{(E_u+\omega_1)^2} \\ &\times [1+n_m(-E_u-\omega_1)], \end{aligned} \tag{B9a}$$

$$\begin{aligned} G_l^{-,(1)} \approx& \frac{\eta_l^2}{2}\Lambda_u(-E_l)n_l(-E_l) \\ &+ \frac{\eta_l^2}{8\pi}\int_{-\infty}^{\infty} \mathrm{d}\,\omega_1 \frac{\Lambda_l(\omega_1)\Lambda_m(E_l+\omega_1)}{(E_l+\omega_1)^2} n_l(\omega_1)n_m(E_l+\omega_1). \end{aligned} \tag{B9b}$$

Similarly, the energies in Figs. B1(d)–B1(f) with the first order correction can be approximated as

$$\begin{aligned} \langle\omega\rangle_{u,+}^{(1)} \approx& \frac{1}{4\pi G_u^+}\Bigg\{2\pi\eta_u^2\Lambda_u(-E_u)[1+n_u(-E_u)](-E_u) \\ &+ \frac{1}{2}\int_{-\infty}^{\infty} \mathrm{d}\,\omega_1 \frac{\Lambda_u(\omega_1)\Lambda_m(-E_u-\omega_1)}{(-E_u-\omega_1)^2}[1+n_m(\omega_1)]\Bigg\}, \end{aligned} \tag{B10a}$$

$$\begin{aligned} \langle\omega\rangle_{l,-}^{(1)} \approx& \frac{1}{4\pi G_l^-}\{2\pi\eta_l^2\Lambda_u(-E_l)n_l(-E_l)(-E_l) \\ &+ \frac{1}{2}\int_{-\infty}^{\infty} \mathrm{d}\,\omega_1 \frac{\Lambda_l(\omega_1)\Lambda_m(E_l+\omega_1)}{(E_l+\omega_1)^2} n_l(\omega_1)n_m(E_l+\omega_1). \end{aligned} \tag{B10b}$$

While the corresponding zeroth order approximation results are

$$\langle\omega\rangle_{u,+}^{(0)} \approx \frac{1}{2G_u^+}\eta_u^2\Lambda_u(-E_u)[1+n_u(-E_u)](-E_u), \tag{B11a}$$

$$\langle\omega\rangle_{l,-}^{(0)} \approx \frac{1}{2G_l^-}\eta_l^2\Lambda_u(-E_l)n_l(-E_l)(-E_l). \tag{B11b}$$

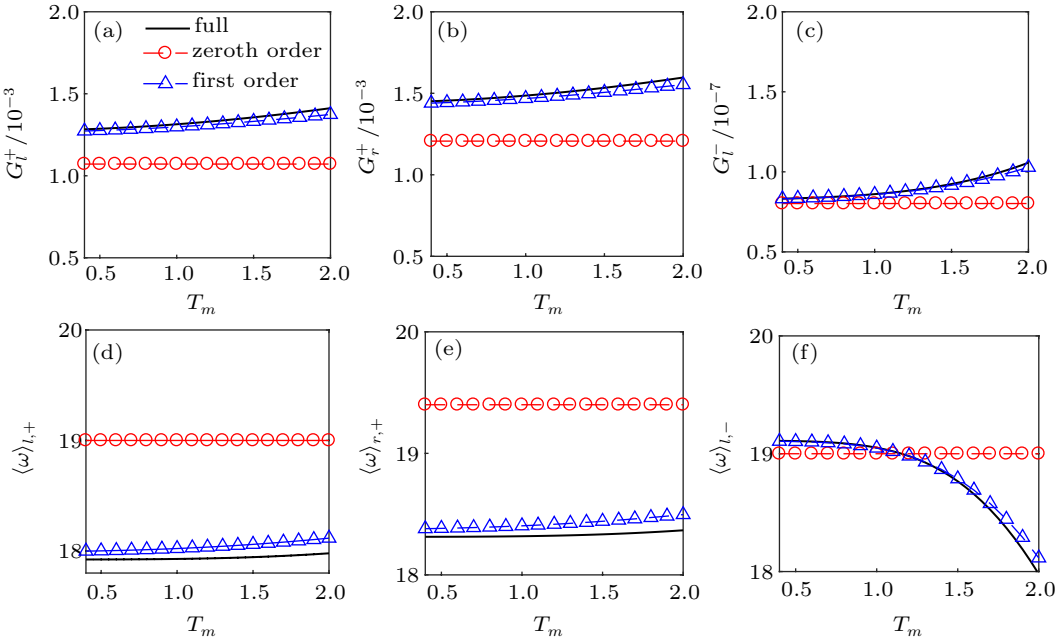

Fig. B1. The transition rates (a) G_l^+, (b) G_r^+, (c) G_l^- and the energy quanta (d) $\langle\omega\rangle_{l,+}$, (e) $\langle\omega\rangle_{r,+}$, (f) $\langle\omega\rangle_{l,-}$ within the nonequilibrium NIBA scheme. The solid black lines represent the full order calculation with expressions shown in Eqs. (13b), (13c), (14a), and (14b); the dashed red lines with circles represent the zeroth order approximation in Eqs. (B8a), (B8b) (B11a), and (B11b); the dashed blue lines with up-triangles represent the first order approximation in Eqs. (B9a), (B9b), (B10a), and (B10b). The other parameters are given by $\varepsilon_l = 1.0$, $\varepsilon_r = 0.6$, $\Delta = 0.6$, $\gamma = 0.0002$, $\omega_c = 10$, $T_l = 2$, and $T_r = 0.4$.

B3. Finite amplification factor at strong coupling

At strong system–middle bath coupling $\alpha_m = 2$, the current into the middle bath is approximated by $J_{m,\mathrm{NIBA}} \approx J_{m,\mathrm{NIBA}}^{(\mathrm{a})} + J_{m,\mathrm{NIBA}}^{(\mathrm{b})}$, with components $J_{m,\mathrm{NIBA}}^{(\mathrm{a})} = G_l^- G_m^- G_r^+(\langle\omega\rangle_{l,-} - \langle\omega\rangle_{r,+})/\mathcal{A}$ and $J_{m,\mathrm{NIBA}}^{(\mathrm{b})} = G^- G_l^+ G_l^-(\langle\omega\rangle_{l,-} - \langle\omega\rangle_{l,+})/\mathcal{A}$, as shown in Eqs. (20a) and (20b). From Fig. B2(a), it is known that for $J_{m,\mathrm{NIBA}}^{(\mathrm{a})}$ the magnitudes of both the flux rate $G_l^- G_m^- G_r^+/\mathcal{A}$ and the energy difference $(\langle\omega\rangle_{l,-} - \langle\omega\rangle_{r,+})$ show monotonic increase, which results in the enhancement of $J_{m,\mathrm{NIBA}}^{(\mathrm{a})}$. Moreover, $J_{m,\mathrm{NIBA}}^{(\mathrm{a})}$

dominates the behavior of $J_{m,\mathrm{NIBA}}$, though $J^{(\mathrm{b})}_{m,\mathrm{NIBA}}$ exhibits the turnover behavior, as shown in Fig. B2(b). While the heat current into the right bath is reduced to $J^{(\mathrm{a})}_{r,\mathrm{NIBA}} \approx \frac{G_l^- G_m^- G_r^+ \langle\omega\rangle_{,r,+}}{\mathcal{A}}$, as given in Eq. (19). And the flux rate $G_l^- G_m^- G_r^+/\mathcal{A}$ and the energy $\langle\omega\rangle_{,r,+}$ are strengthened by increasing temperature T_m. Hence, $J_{r,\mathrm{NIBA}}$ shows the monotonic increase as in Fig. B2(c). considering the large deviation of magnitudes of currents $J_{r,\mathrm{NIBA}}$ and $J_{m,\mathrm{NIBA}}$, the large and finite heat amplification β_r is expected to be observed.

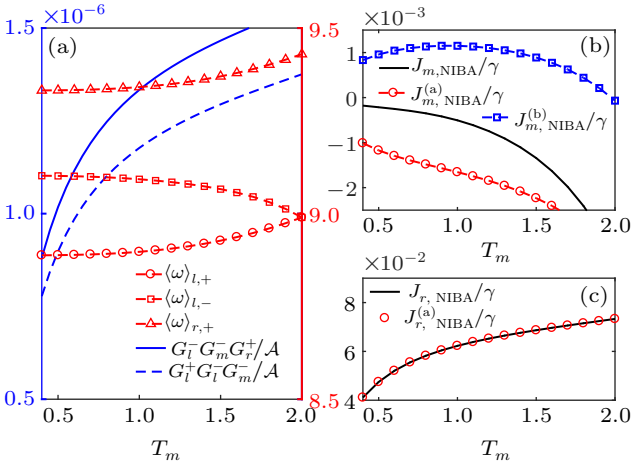

Fig. B2. (a) Average energy quanta $\langle\omega\rangle_{l,\pm}$, $\langle\omega\rangle_{r,+}$, and the flux rates $G_l^- G_m^- G_r^+/\mathcal{A}$ and $G_l^+ G_l^- G_m^-/\mathcal{A}$; (b) heat current into the middle bath $J_{m,\mathrm{NIBA}}/\gamma$, the main components $J^{(\mathrm{a})}_{m,\mathrm{NIBA}}/\gamma$ and $J^{(\mathrm{b})}_{m,\mathrm{NIBA}}/\gamma$; (c) heat current into the right bath $J_{r,\mathrm{NIBA}}/\gamma$ and the main component $J^{(\mathrm{a})}_{r,\mathrm{NIBA}}/\gamma$ within the nonequilibrium NIBA scheme at strong coupling $\alpha_m = 2$. The other parameters are given by $\varepsilon_l = 1.0$, $\varepsilon_r = 0.6$, $\Delta = 0.6$, $\gamma = 0.0002$, $\omega_c = 10$, $T_l = 2$, and $T_r = 0.4$.

Appendix C: Redfield scheme

The Hamiltonian of the three-level system is given by $\hat{H}_s = \sum_{u=l,r}\varepsilon_u|u\rangle\langle u| + \Delta(|l\rangle\langle r| + \mathrm{H.c.})$. The two excited eigenstates are given by $|+\rangle = \cos\frac{\theta}{2}|l\rangle + \sin\frac{\theta}{2}|r\rangle$ and $|-\rangle = -\sin\frac{\theta}{2}|l\rangle + \cos\frac{\theta}{2}|r\rangle$, with $\tan\theta = \Delta/\delta\varepsilon$, the eigenenergy $E_\pm = \bar{\varepsilon} \pm \sqrt{\delta\varepsilon^2 + \Delta^2}$, $\bar{\varepsilon} = (\varepsilon_l + \varepsilon_r)/2$ and $\delta\varepsilon = (\varepsilon_l - \varepsilon_r)/2$. The system–phonon interaction is given by $\hat{V}_m = \sum_k (g_{k,m}\hat{b}^\dagger_{k,m} + \mathrm{H.c.}) \otimes \hat{S}_m$, with $\hat{S}_m = \cos\theta(|+\rangle\langle+| - |-\rangle\langle-|) - \sin\theta(|+\rangle\langle-| + |-\rangle\langle+|)$. Then, the dynamical equation is given by

$$\frac{\mathrm{d}\hat{\rho}_\chi}{\mathrm{d}t} = -\mathrm{i}[\hat{H}_s, \hat{\rho}_\chi] + \sum_u \mathcal{L}^u_{\chi_u}[\hat{\rho}_\chi], \tag{C1}$$

where the dissipator related with the middle bath is

$$\begin{aligned}\mathcal{L}^{\chi_m}_m[\hat{\rho}_\chi] = \sum_{\omega,\omega'} \{&-J_m(\omega')n_m(\omega')[\hat{\rho}_\chi \hat{S}_m(\omega')\hat{S}_m(\omega) + \mathrm{H.c.}] \\ &+ \mathrm{e}^{-\mathrm{i}\omega'\chi_m} J_m(\omega')n_m(\omega')\hat{S}_m(\omega)\hat{\rho}_\chi \hat{S}_m(\omega') \\ &+ \mathrm{e}^{\mathrm{i}\omega'\chi_m} J_m(\omega')[1 + n_m(\omega')]\hat{S}_m(\omega')\hat{\rho}_\chi \hat{S}_m(\omega)\},\end{aligned} \tag{C2}$$

with $\hat{S}_m(-\tau) = \sum_\omega \hat{S}_m(\omega)\mathrm{e}^{\mathrm{i}\omega\tau}$. And the dissipator related with the $l(r)$-th bath is

$$\begin{aligned}\mathcal{L}^u_{\chi_u}[\hat{\rho}_{\{\chi\}}] =& \frac{J_u(\omega')}{4} n_u(\omega')\mathrm{e}^{-\mathrm{i}\omega'\chi_u}\big[\hat{Q}^\dagger_u(\omega')\hat{\rho}_{\{\chi\}}\hat{Q}_u(\omega) \\ &+ \hat{Q}^\dagger_u(\omega)\hat{\rho}_{\{\chi\}}\hat{Q}_u(\omega')\big] \\ &+ \frac{J_u(\omega')}{4}(1 + n_u(\omega'))\mathrm{e}^{\mathrm{i}\omega'\chi_u}\big[\hat{Q}_u(\omega')\hat{\rho}_{\{\chi\}}\hat{Q}^\dagger_u(\omega) \\ &+ \hat{Q}_u(\omega)\hat{\rho}_{\{\chi\}}\hat{Q}^\dagger_u(\omega')\big] \\ &- \Big[\frac{J_u(\omega')}{4} n_u(\omega')\hat{Q}_u(\omega)\hat{Q}^\dagger_u(\omega')\hat{\rho}_{\{\chi\}} \\ &+ \frac{J_u(\omega')}{4}(1 + n_u(\omega'))\hat{Q}^\dagger_u(\omega)\hat{Q}_u(\omega')\hat{\rho}_{\{\chi\}} + \mathrm{H.c.}\Big],\end{aligned} \tag{C3}$$

with $\hat{S}_u(-\tau) = \sum_\omega \hat{Q}_u(\omega)\mathrm{e}^{\mathrm{i}\omega\tau}$.

The steady state heat current obtained by FCS is given by

$$\begin{aligned}J_l =& \frac{\cos^2\frac{\theta}{2}}{2}\kappa^a_{l,+}E_+\rho_{++} + \frac{\sin^2\frac{\theta}{2}}{2}\kappa^a_{l,-}E_-\rho_{--} \\ &- \Big(\frac{\cos^2\frac{\theta}{2}}{2}\kappa^e_{l,+}E_+ + \frac{\sin^2\frac{\theta}{2}}{2}\kappa^e_{l,-}E_-\Big)\rho_{00},\end{aligned} \tag{C4}$$

$$\begin{aligned}J_r =& \frac{\sin^2\frac{\theta}{2}}{2}\kappa^a_{r,+}E_+\rho_{++} + \frac{\cos^2\frac{\theta}{2}}{2}\kappa^a_{r,-}E_-\rho_{--} \\ &- \Big(\frac{\sin^2\frac{\theta}{2}}{2}\kappa^e_{r,+}E_+ + \frac{\cos^2\frac{\theta}{2}}{2}\kappa^e_{r,-}E_-\Big)\rho_{00},\end{aligned} \tag{C5}$$

$$J_m = \frac{\sin^2\theta}{2}(E_+ - E_-)(\kappa^a_m\rho_{++} - \kappa^e_m\rho_{--}), \tag{C6}$$

and $J_m = -J_l - J_r$. It should be noted that the steady state coherence in the eigenbasis is negligible.

Moreover, the steady state populations are given by

$$P_+ = \frac{1}{\mathcal{B}}(\Gamma^e_+ + \Gamma^e_-)[\Gamma^e_+\Gamma^a_- + (\Gamma^e_+ + \Gamma^e_-)\Gamma^+_p], \tag{C7a}$$

$$P_- = \frac{1}{\mathcal{B}}(\Gamma^e_+ + \Gamma^e_-)[\Gamma^a_+\Gamma^e_- + (\Gamma^e_+ + \Gamma^e_-)\Gamma^-_p], \tag{C7b}$$

$$\begin{aligned}P_m =& \frac{1}{\mathcal{B}}\big(\Gamma^a_+[\Gamma^e_+\Gamma^a_- + (\Gamma^e_+ + \Gamma^e_-)\Gamma^+_p] \\ &+ \Gamma^a_-[\Gamma^a_+\Gamma^e_- + (\Gamma^e_+ + \Gamma^e_-)\Gamma^-_p]\big),\end{aligned} \tag{C7c}$$

$$\begin{aligned}\mathcal{B} =& (\Gamma^a_+ + \Gamma^e_+ + \Gamma^e_-)[\Gamma^e_+\Gamma^a_- + (\Gamma^e_+ + \Gamma^e_-)\Gamma^+_p] \\ &+ (\Gamma^a_- + \Gamma^e_+ + \Gamma^e_-)[\Gamma^a_+\Gamma^e_- + (\Gamma^e_+ + \Gamma^e_-)\Gamma^-_p],\end{aligned} \tag{C7d}$$

where the rates are defined as $\Gamma^{e(a)}_+ = \frac{1}{2}(\kappa^{e(a)}_{l,+}\cos^2\frac{\theta}{2} + \kappa^{e(a)}_{r,+}\sin^2\frac{\theta}{2})$, $\Gamma^{e(a)}_- = \frac{1}{2}(\kappa^{e(a)}_{l,-}\sin^2\frac{\theta}{2} + \kappa^{e(a)}_{r,-}\cos^2\frac{\theta}{2})$, and $\Gamma^{+(-)}_p = \frac{\sin^2\theta}{8}\kappa^{e(a)}_p$, with $\kappa^e_{u,\pm} = \Lambda_u(E_\pm)n_u(E_\pm)$, $\kappa^a_{u,\pm} = \Lambda_u(E_\pm)[1 + n_u(E_\pm)]$, $\kappa^e_p = \Lambda_m(E_+ - E_-)n_m(E_+ - E_-)$, and $\kappa^e_p = \Lambda_m(E_+ - E_-)[1 + n_m(E_+ - E_-)]$. The currents are specified as

$$\begin{aligned}J_l =& \sum_{\xi=\pm}\frac{(1 + \xi\cos\theta)}{4\mathcal{B}}E_\xi\big[\kappa^a_{l,\xi}(\Gamma^e_+ + \Gamma^e_-)\Gamma^e_\xi\Gamma^a_{\bar{\xi}} \\ &- \kappa^e_{l,\xi}(\Gamma^a_+\Gamma^e_+\Gamma^a_- + \Gamma^a_-\Gamma^e_-\Gamma^a_+)\big] \\ &+ \sum_{\xi=\pm}\frac{(1 + \xi\cos\theta)}{4\mathcal{B}}E_\xi(\Gamma^e_+ + \Gamma^e_-)\big[\kappa^a_{l,\xi}(\Gamma^e_+ + \Gamma^e_-)\Gamma^\xi_p\end{aligned}$$

$$-\kappa^e_{l,\xi}(\Gamma^a_+\Gamma^+_p+\Gamma^a_-\Gamma^-_p)\big], \tag{C8}$$

$$J_r=\sum_{\xi=\pm}\frac{(1-\xi\cos\theta)}{4\mathcal{B}}E_\xi\big[\kappa^a_{r,\xi}(\Gamma^e_++\Gamma^e_-)\Gamma^e_\xi\Gamma^a_\xi - \kappa^e_{r,\xi}(\Gamma^a_+\Gamma^e_+\Gamma^a_-+\Gamma^a_-\Gamma^e_-\Gamma^a_+)\big] + \sum_{\xi=\pm}\frac{(1-\xi\cos\theta)}{4\mathcal{B}}E_\xi(\Gamma^e_++\Gamma^e_-)\big[\kappa^a_{r,\xi}(\Gamma^e_++\Gamma^e_-)\Gamma^\sigma_p - \kappa^e_{r,\sigma}(\Gamma^a_+\Gamma^+_p+\Gamma^a_-\Gamma^-_p)\big]. \tag{C9}$$

The current into the middle bath is

$$J_m=-\frac{1}{\mathcal{B}}(E_+-E_-)(\Gamma^e_++\Gamma^e_-)(\Gamma^a_+\Gamma^e_-\Gamma^+_p-\Gamma^a_-\Gamma^e_+\Gamma^-_p). \tag{C10}$$

In particular, under the condition $E_+\gg E_-$ and $\Gamma^\pm_p\gg\Gamma^{a(e)}_-$, the coefficient $\mathcal{B}$ is reduced to $\mathcal{B}=(\Gamma^e_++\Gamma^-_e)[(\Gamma^a_++\Gamma^e_++\Gamma^e_-)\Gamma^+_p+(\Gamma^a_-\Gamma^e_++\Gamma^e_-)\Gamma^-_p]$, and the currents into the middle and right baths are approximated as

$$J_m\approx-\frac{E_+(\Gamma^e_++\Gamma^e_-)}{\mathcal{B}}(\Gamma^a_+\Gamma^e_-\Gamma^+_p-\Gamma^a_-\Gamma^e_+\Gamma^-_p), \tag{C11}$$

$$J_r\approx\frac{(1-\cos\theta)E_+(\Gamma^e_++\Gamma^e_-)}{4\mathcal{B}}\times\big[\kappa^a_{r,+}(\Gamma^e_++\Gamma^e_-)\Gamma^+_p-\kappa^e_{r,+}(\Gamma^a_+\Gamma^+_p+\Gamma^a_-\Gamma^-_p)\big]. \tag{C12}$$

If we redefine $J_m=J'_m+J^0_m$ and $J_r=J'_r+J^0_r$, with

$$J'_m=E_+\times\frac{\Gamma^a_-\Gamma^e_+}{(\Gamma^a_-+\Gamma^e_++\Gamma^e_-)}\times\frac{(\Gamma^a_+\Gamma^e_-)/(\Gamma^a_-\Gamma^e_+)+(\Gamma^a_++\Gamma^e_++\Gamma^e_-)/(\Gamma^a_-+\Gamma^e_++\Gamma^e_-)}{\Gamma^-_p/\Gamma^+_p+(\Gamma^a_++\Gamma^e_++\Gamma^e_-)/(\Gamma^a_-+\Gamma^e_++\Gamma^e_-)}, \tag{C13}$$

$$J'_r=\frac{(1-\cos\theta)E_+}{4}\times\frac{\kappa^e_{r,+}\Gamma^a_-}{(\Gamma^a_-+\Gamma^e_++\Gamma^e_-)}\times\frac{(\Gamma^a_++\Gamma^e_++\Gamma^e_-)/(\Gamma^a_-+\Gamma^e_++\Gamma^e_-)+[\kappa^a_{r,+}(\Gamma^e_++\Gamma^e_-)-\kappa^e_{r,+}\Gamma^a_+]/(\kappa^e_{r,+}\Gamma^a_-)}{\Gamma^-_p/\Gamma^+_p+(\Gamma^a_++\Gamma^e_++\Gamma^e_-)/(\Gamma^a_-+\Gamma^e_++\Gamma^e_-)}, \tag{C14}$$

$J^0_m=E_+\Gamma^a_-\Gamma^e_+/(\Gamma^a_-+\Gamma^e_++\Gamma^e_-)$, and $J^0_r=-\frac{(1-\cos\theta)E_+}{4}\kappa^e_{r,+}\Gamma^a_-/(\Gamma^a_-+\Gamma^e_++\Gamma^e_-)$. It should be noted that J^0_m and J^0_r are irrelevant to T_m. Hence, the linear heat amplification is given by

$$\beta_r\approx\frac{(1-\cos\theta)}{4}\left|\frac{\kappa^e_{r,+}\Gamma^a_-(\Gamma^a_++\Gamma^e_++\Gamma^e_-)+(\Gamma^a_-+\Gamma^e_++\Gamma^e_-)[\kappa^a_{r,+}(\Gamma^e_++\Gamma^e_-)-\kappa^e_{r,+}\Gamma^a_+]}{\Gamma^a_-\Gamma^e_+(\Gamma^a_++\Gamma^e_++\Gamma^e_-)+(\Gamma^a_-+\Gamma^e_++\Gamma^e_-)\Gamma^a_+\Gamma^e_-}\right|. \tag{C15}$$

Moreover, considering the condition $\Gamma^{a(e)}_+\gg\Gamma^{a(e)}_-$, the amplification factor is simplified as

$$\beta_r\approx\frac{\sin^2\theta}{16}\left|\frac{\kappa^e_{l,+}\kappa^a_{r,+}-\kappa^a_{l,+}\kappa^e_{r,+}}{\Gamma^a_-(\Gamma^a_++\Gamma^e_+)+\Gamma^a_+\Gamma^e_-}\right|. \tag{C16}$$

References

[1] Clausius R 1879 *The Mechanical Theory of Heat* (London: MacMillan)
[2] Esposito M, Ochoa M A and Galperin M 2015 *Phys. Rev. Lett.* **114** 080602
[3] Katz G and Kosloff R 2016 *Entropy* **18** 186
[4] Chen X B and Duan W H 2015 *Acta Phys. Sin.* **64** 186302 (in Chinese)
[5] Benenti G, Casati G, Saito K and Whitney R S 2017 *Phys. Rep.* **694** 1
[6] Segal D 2008 *Phys. Rev. Lett.* **101** 260601
[7] Ren J, Hanggi P and Li B 2010 *Phys. Rev. Lett.* **104** 170601
[8] Micadei K, Peterson J P S, Souza A M, Sarthour R S, Oliveira I S, Landi G T, Batalhao T B, Serra R M and Lutz E 2019 *Nat. Comm.* **10** 2456
[9] Wang L and Li B 2007 *Phys. Rev. Lett.* **99** 177208
[10] Cui L, Jeong W H, Hur S H, Matt M, Klockner J C, Pauly F, Nielaba P, Cuevas J C, Meyhofer E and Reddy P 2017 *Science* **355** 1192
[11] Segal D 2017 *Science* **355** 1125
[12] Li B 2006 *Appl. Phys. Lett.* **88** 143501
[13] Li N B, Ren J, Wang L, Zhang G, Hanggi P and Li B 2012 *Rev. Mod. Phys.* **84** 1045
[14] He D H, Buyukdagli S and Hu B 2009 *Phys. Rev. B* **80** 104302
[15] He D H, Ai B Q, Chan H K and Hu B 2010 *Phys. Rev. E* **81** 041131
[16] Chan H K, He D H and Hu B 2014 *Phys. Rev. E* **89** 052126
[17] Joulain K, Drevillon K, Ezzahri Y and Ordonez-Miranda J 2016 *Phys. Rev. Lett.* **116** 200601
[18] Guo B Q, Liu T and Yu C S 2018 *Phys. Rev. E* **98** 022118
[19] Guo B Q, Liu T and Yu C S 2019 *Phys. Rev. E* **99** 032112
[20] Du J Y, Sheng W, Su S H and Chen J C 2019 *Phys. Rev. E* **99** 062123
[21] Wang C, Chen X M, Sun K W and Ren J 2018 *Phys. Rev. A* **97** 052112
[22] Liu H, Wang C, Wang L Q and Ren J 2019 *Phys. Rev. E* **99** 032114
[23] Jiang J H, Kulkarni M, Segal D and Imary Y 2015 *Phys. Rev. B* **92** 045309
[24] Su S H, Zhang Y C, Andresen B and Chen J C arXiv:1811.02400
[25] Scovil H E D and Schulz-DuBois E O 1959 *Phys. Rev. Lett.* **2** 262
[26] Quan H T, Liu Y X, Sun C P and Nori F 2007 *Phys. Rev. E* **76** 031105
[27] Boukobza E and Tannor D J 2007 *Phys. Rev. Lett.* **98** 240601
[28] Krause T, Brandes T, Esposito M and Shaller G 2015 *J. Chem. Phys.* **142** 134106
[29] Xu D Z, Wang C, Zhao Y and Cao J 2016 *New J. Phys.* **18** 023003
[30] Li S W, Kim M B, Agarwal G S and Scully M O 2017 *Phys. Rev. A* **96** 063806
[31] Segal D 2018 *Phys. Rev. E* **97** 052145
[32] Kilgour M and Segal D 2018 *Phys. Rev. E* **98** 012117
[33] Friedman H M and Segal D 2019 *Phys. Rev. E* **100** 062112
[34] Wang C, Ren J and Cao J 2015 *Sci. Rep.* **5** 11787
[35] Wang C, Ren J and Cao J 2017 *Phys. Rev. A* **95** 023610
[36] Segal D and Nitzan A 2005 *Phys. Rev. Lett.* **94** 034301
[37] Segal D 2006 *Phys. Rev. B* **73** 205415
[38] Nicolin L and Segal D 2011 *J. Chem. Phys.* **135** 164106
[39] Nicolin L and Segal D 2011 *Phys. Rev. B* **84** 161414
[40] Scully M O and Zubairy M S 1997 *Quantum Optics* (Cambridge: Cambridge University Press)
[41] Tscherbul T V and Brumer P 2014 *Phys. Rev. Lett.* **113** 113601
[42] Leggett A J, Chakravarty S, Dorsey A T, Fisher M P A, Garg A and Zwerger W 1987 *Rev. Mod. Phys.* **59** 1
[43] Jang Seogjoo , Berkelbach T C and Reichman D 2013 *New J. Phys.* **15** 105020
[44] Nazir A 2009 *Phys. Rev. Lett.* **103** 146404
[45] Xu D Z and Cao J 2016 *Frontiers of Physics* **11** 110308
[46] Qin M, Wang C Y, Cui H T and Yi X X 2019 *Phys. Rev. A* **99** 032111
[47] The component frequencies are given by $\omega=\{0,\pm\Lambda\}$, $\Lambda=2\sqrt{(\delta\varepsilon)^2+(\eta\Delta)^2}$. For $\alpha=x$, the projecting operators are $\hat{P}_x(0)=\sin\theta(|+\rangle\langle+|-|-\rangle\langle-|)$, $\hat{P}_x(\Lambda)=\cos\theta|-\rangle\langle+|$, and $\hat{P}_x(-\Lambda)=[\hat{P}_x(\Lambda)]^\dagger$. While for $\alpha=y$, the operators become $\hat{P}_y(0)=0$, $\hat{P}_y(\Lambda)=\mathrm{i}$, and $\hat{P}_y(-\Lambda)=-\mathrm{i}$.
[48] The component frequencies are given by $\omega=\{E_+,E_-\}$ with $E_+=\bar{\varepsilon}+\sqrt{(\delta\varepsilon)^2+(\eta\Delta)^2}$ and $E_-=\bar{\varepsilon}-\sqrt{(\delta\varepsilon)^2+(\eta\Delta)^2}$. For $u=l$, the projecting operators are $\hat{S}_l(E_+)=\cos\frac{\theta}{2}|0\rangle\langle+|$ and $\hat{S}_l(E_-)=-\sin\frac{\theta}{2}|0\rangle\langle-|$. While for $u=r$, the operators are $\hat{S}_r(E_+)=\sin\frac{\theta}{2}|0\rangle\langle+|$ and $\hat{S}_r(E_-)=\cos\frac{\theta}{2}|0\rangle\langle-|$.
[49] Friedman H M, Agarwalla B K and Segal D 2018 *New J. Phys.* **20** 083026